Diploma thesis

Exploring chemical contrast on cellulosic materials with atomic force microscopy

by

Caterina Czibula

at the Institute of Physics

Montanuniversität Leoben, Austria

under supervision of

Ao. Univ. Prof. Dr. Christian Teichert

Dipl.-Ing. Dr. mont. Christian Ganser

refereed by

Ao. Univ. Prof. Dr. Christian Teichert

Leoben, June 2016

Dedicated to my grandparents

Eidesstattliche Erklärung

Ich erkläre an Eides statt, dass ich diese Arbeit selbstständig verfasst, andere als die angegebenen Quellen und Hilfsmittel nicht benutzt und mich auch sonst keiner unerlaubten Hilfsmittel bedient habe.

Affidavit

I declare in lieu of oath, that I wrote this thesis and performed the associated research myself, using only literature cited in this volume.

_____

Caterina Czibula
Leoben, June 2016

Abstract

During papermaking and the production of regenerated cellulose fibers, hemicelluloses - such as xylan - are extracted. Like cellulose, the hemicelluloses are polysaccharides, but are – in contrast to the linear cellulose molecule – highly branched. So far, the utilization of the extracted hemicelluloses is limited. However, it has been reported that applying xylan as an additive to paper has a positive influence to the mechanical properties of paper. To understand the nature of this enhancement, the interaction between cellulose and xylan needs to be studied in detail.

The goal of this work was to explore whether xylan can be selectively localized on the fiber surfaces. However, paper fibers are an inhomogeneous and complicated hierarchical system. Therefore, in this work, the adsorption of xylan to amorphous cellulose thin films was studied as a first step. Different model films were prepared on quartz-crystal-microbalance substrates and afterwards exposed to a solution of xylan with different filters, ionic strengths, and pH. In the final part of this work, also paper fibers with adsorbed xylan were investigated. Atomic force microscopy (AFM) was employed to characterize the surface topography of films and fibers. To obtain chemical contrast between cellulose and xylan, OH- and CH_3-functionalized AFM tips were used. If the functionalized tip would interact differently with xylan than it does with cellulose, a phase shift in tapping mode AFM would occur, allowing to distinguish xylan from the cellulose background. By also employing so-called AFM force mapping, the spatially resolved adhesion force between functionalized tip and surface can be recorded.

The results for the cellulose/xylan thin films showed that the specific surface features are changing with varying ionic strength (0, 1 and 100 mmol NaCl) and pH (7, 8 and 9). These features can be either elongated, spherical, or dot-like. The elongated structures are located along the slope of the hills, but the others prefer to adsorb mostly on top of the film's hill-like structure. Paper fibers are much rougher than the model thin films. Their surfaces look wrinkled and microfibrils and fibril bundles are visible. Here, xylan seems to adsorb as nearly spherical features with a diameter of about 100 nm and 20 nm – 30 nm in height.

For the chemical investigation with OH- and CH_3-functionalized probes, cellulose/xylan films as well as paper fibers showed a contrast in phase as well as in force maps. Since both functionalizations – although chemically different – showed the same contrast, it is likely that there is a topographic influence. In addition, it was observed that a phase or adhesion contrast always corresponded to a change in topography. Although a clear chemical contrast could not be verified between cellulose and xylan, the investigation brought important insight into the established AFM methods and provided a better understanding of probe-sample surface interaction.

Kurzfassung

Während der Papiererzeugung und der Produktion von regenerierten Cellulosefasern werden Hemicellulosen, wie zum Beispiel Xylan, extrahiert. Genauso wie Cellulose sind Hemicellulosen zwar auch Polysaccharide, aber – im Gegensatz zu dem linearen Cellulosemolekül – stark verzweigt. Bislang ist die Verwendung der extrahierten Hemicellulose gering. Es wird aber berichtet, dass die Zugabe von Xylan als Papieradditiv einen positiven Einfluss auf die mechanischen Eigenschaften von Papier haben soll. Um die Natur dieser Verbesserung zu verstehen, muss die Wechselwirkung zwischen Cellulose und Xylan besser im Detail untersucht werden.

Das Ziel dieser Arbeit war herauszufinden, ob Xylan gezielt auf den Faseroberflächen lokalisiert werden kann. Papierfasern sind aber ein inhomogenes und kompliziertes hierarchisches System. Daher wurde in dieser Arbeit zuerst die Adsorption von Xylan auf amorphen Cellulose-Dünnfilmen untersucht. Verschiedene Modellfilme wurden auf Substraten für Quartzkristall-Mikrowaagen präpariert und anschließend einer Lösung von Xylan ausgesetzt, wobei die Filtrierung, die Ionenstärke und der pH-Wert variiert wurden. Im letzten Teil dieser Arbeit wurden auch Papierfasern mit adsorbiertem Xylan untersucht. Rasterkraftmikroskopie (AFM) wurde angewendet, um die Topographie der Filme und Fasern zu charakterisieren. Um einen chemischen Kontrast zwischen Cellulose und Xylan zu erhalten, wurden OH- und CH_3-funktionalisierte Spitzen verwendet. Falls die funktionalisierte Spitze mit Xylan anders wechselwirkt als mit Cellulose, würde das zu einer Phasenverschiebung in Tapping Mode AFM führen, was erlaubt, Xylan vom Cellulose-Hintergrund zu unterscheiden. Mit der zusätzlichen Anwendung von sogenanntem „AFM Force Mapping“ kann die räumlich aufgelöste Adhäsionskraft zwischen funktionalisierter Spitze und Oberfläche aufgenommen werden.

Die Resultate für Cellulose/Xylan Dünnfilme zeigen, dass sich die Form der Oberflächenstrukturen mit unterschiedlicher Ionenstärke (0, 1 und 100 mmol NaCl) und unterschiedlichem pH-Wert (7, 8 und 9) ändern. Diese Strukturen sind länglich, kugelig oder punktartig. Die länglichen Strukturen sind an der Neigung von Hügeln zu finden, während die anderen Strukturen aber hauptsächlich oben auf den hügeligen Filmstrukturen adsorbieren. Papierfasern sind viel rauer als Modelldünnfilme. Ihre Oberfläche sieht faltig aus, und man kann Mikrofibrillen und Fibrillenbündel sehen. Hier scheint Xylan als beinahe sphärische Struktur zu adsorbieren, mit einem Durchmesser von ungefähr 100 nm und 20 nm – 30 nm Höhe.

Bei der chemischen Untersuchung mit OH- und CH_3-funktionalisierten Sonden zeigten sowohl Cellulose/Xylan Filme als auch Papierfasern einen Kontrast in der Phase und in Adhäsion. Da aber beide Funktionalisierungen, obwohl sie von verschiedener chemischer

Natur sind, denselben Kontrast zeigen, ist es möglich, dass es einen Topographieeinfluss gibt. Zusätzlich konnte festgestellt werden, dass es zu Phasen- oder Adhäsionskontrast immer eine dazugehörige Änderung in der Topographie gegeben hat. Obwohl ein klarer chemischer Kontrast nicht nachgewiesen werden konnte, brachten die Untersuchungen wichtige Einsicht in die etablierten AFM Methoden und lieferten ein besseres Verständnis für die Wechselwirkung zwischen Spitze und Probenoberfläche.

Acronyms

σ	root mean square (RMS) roughness
ξ	lateral correlation length
α	Hurst parameter
1D	one-dimensional
AFM	atomic force microscopy
F_{ad}	adhesion force
HHCF	height height correlation function
JOC	jump-off-contact
JTC	jump-to-contact
k_c	spring constant
ML	middle lamella
P	primary wall
px	pixel
QCM	quartz crystal microbalance
S1	secondary wall 1
S2	secondary wall 2
S3	secondary wall 3
T	tertiary wall
TMSC	Trimethylsilyl cellulose

Contents

1 Motivation

Xylan is the predominant hemicellulose in plants and wood [1]. It is a byproduct in papermaking and within the fabrication of regenerated cellulose fibers. During the pulp and paper production, most of the xylan is dissolved from the wood matrix. The interactions of hemicelluloses like xylan with cellulosic substrates have recently attracted considerable interest, both from basic and applied research [2, 3]. High hemicellulose content in fibers may be beneficial for recycling purposes because it may lead to lower tendency to hornify in drying [4]. Also, a higher hemicellulose content might be responsible for a more porous surface structure of kraft pulp fibers [5]. It was found that as the amount of hemicelluloses decreased, so did mechanical properties [6]. Additionally, it was proposed that the removal of xylan from hardwood may decrease the fiber strength [7]. Xylan's ability to positively influence the mechanical properties of paper might open a pathway for additional industrial use of this hemicellulose. For this purpose, the interaction between cellulose and xylan has to be understood in detail. The goal of this work was to explore whether xylan can be selectively localized on the surface of cellulose model films and finally also on cellulose fibers.

Atomic force microscope (AFM) was employed to characterize the topography of amorphous cellulose thin films and paper fibers with adsorbed xylan. On cellulosic surfaces, xylan is often observed in particle-like aggregates [8]. Here, its adsorption behavior was closer studied in detail with modified filtering, ionic strength, and pH. Especially amorphous thin films have become useful to get better insights into cellulosic materials. In this work, cellulose/xylan model films played an important role to study two AFM methods for obtaining chemical contrast between xylan and cellulose.

To really achieve a chemical contrast, hydrophilic OH- and hydrophobic CH_3-functionalized probes were employed during AFM phase contrast imaging and AFM force mapping. In phase contrast, the phase shift between excitation and the detected oscillation of the cantilever in tapping mode provides a material's contrast because of a difference in energy dissipation. With force mapping, it is possible to record the adhesion force locally. This technique allows also to extract mechanical properties and is commonly applied to biomaterials and even biological samples [9]. Combining both methods to obtain chemical surface information on cellulose and xylan is a novel approach.

2 Theoretical background

2.1 Cellulosic materials, hemicellulose and properties

2.1.1 Cellulose

Cellulose is a polysaccharide consisting of a linear chain of β-(1, 4)-linked D-glucose units [10]. It is the most abundant organic polymer on earth [11] and an important structural component of the fiber cell wall in plants. In figure 2.1 the structure of cellulose with chair confirmation of the glucose unit is presented.

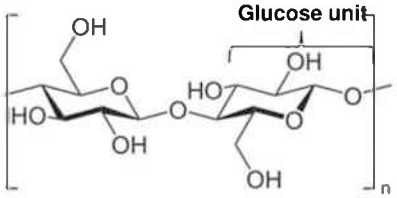

Figure 2.1: Structure of the cellulose chain [12].

2.1.2 Xylan

Xylan is the most frequent group of hemicellulose in wood with 10% to 35% of the total mass [1]. The main chain of xylan consists of xylose units, which are covalently linked by β-(1, 4)-glycosidic bonds [13].

Compared to cellulose, the hemicellulose polymer has a branched structure. Hemicellulose can also contain different sugar monomers beside glucose. These sugar components are classified into pentoses (β-D-xylose, α-L-arabinopyranose, α-L-arabinofuranose); hexoses (β-D-glucose, β-D-mannose, α-D-galactose), hexuranic acids (α-D-4-O-methylglucuronic acid) and deoxy-hexoses [14]. In figure 2.2, a possible structure of xylan is presented.

Hemicelluloses have an important influence on the properties of pulp and paper, especially mechanical strength.

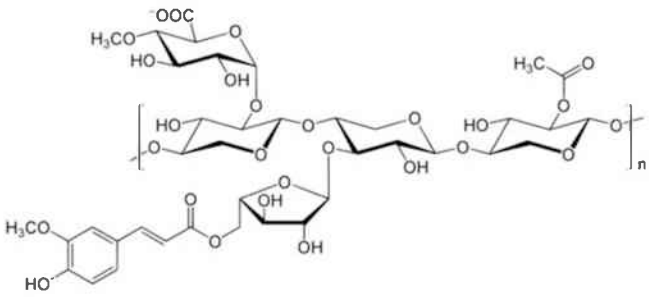

Figure 2.2: Structure of xylan [15].

2.1.3 Cell wall structure of wood fibers

The main components of the fiber cell wall are cellulose, hemicellulose and lignin, which is a highly branched polymer that acts like a glue between the fibers. A model of the cell wall is shown in figure 2.3.

Depending on the alignment of cellulose fibrils and the chemical composition, the cell wall consists of different layers.

The primary wall (P) consists of randomly oriented microfibrils and high amounts of lignin. On its inner side, it is bordered by the secondary wall number one (S1), the secondary wall number two (S2) and the secondary wall number three (S3). All three layers of the secondary wall show an orientation of the microfibrils and decreasing lignin content from S1 to S3. The S2 is the thickest layer and contributes the most to the physical and mechanical properties of a fiber [16]. The middle lamella (ML) borders the P layer on the outside and glues the individual cells together. In the center of the fiber is a hollow part called lumen, where water and nutrients are transported.

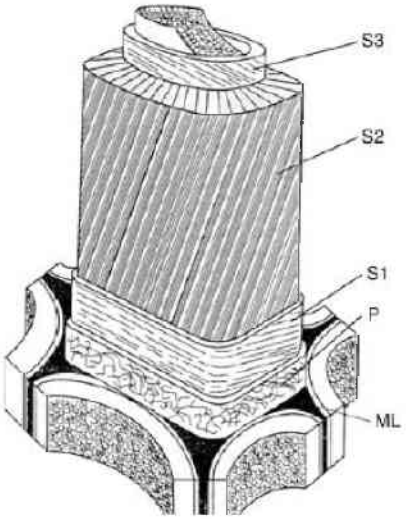

Figure 2.3: Layers of the fiber cell wall [17].

2.1.4 Reactions of xylan during chemical pulping

For the production of paper, fibers undergo a chemical process called kraft pulping. Its main purpose is the removal of the lignin-rich middle lamella and lignin from the cell wall layers. The decomposition of the ML results in fiber separation [13]. During the delignification, xylan is also dissolved. Changes in the chemical structure of xylan affect its solubility and the adsorption behavior on the surface [14].

2.1.5 Adsorption of xylan

The adsorption of xylan is a very slow physical process driven by Van der Waals forces and hydrogen bonds between the hydroxyl (-OH) groups of cellulose and xylan [10, 11].

Xylan adsorbs on a cellulose surface in a four step process: First, xylan has to diffuse to the cellulose surface through the solution. Next, it needs to adsorb to the surface. Third, it is also possible that small molecules diffuse into the cellulosic material. Step four is the reverse of the whole mechanism [20].

There is a strong influence of xylan composition. The adsorption of xylan on cellulosic surfaces depends on the molecular weight, side groups of the xylan, the origin, and extraction method [21]. Less side groups are favorable for adsorption. This observation has many explanations including lower solubility of the xylan adsorbate [22], a reduced steric repulsion between xylan and cellulose [22], dehydration of xylan [21] and a higher interaction between xylan molecules [8].

Also, one has to consider the influence of the pH value and the ionic strength. At lower pH, e.g. at the end of the kraft pulping [21], more xylan is adsorbed. This behavior is discussed as a decrease in solubility [13, 14] and in electrostatic repulsion between hydroxyl and carboxyl (-COOH) groups [22]. An increase of the ionic strength also reduces electrostatic repulsion between the hydroxyl and carboxyl groups of xylan and the hydroxyl groups of cellulose [22].

2.2 Atomic force microscopy – measurement principle

In this work, the method atomic force microscopy (AFM) [23] has been employed to obtain nanometer scale information on the topography. The principle of AFM is rather simple, a sharp tip at the end of a cantilever scans across a surface. The tip movement relative to the surface in lateral directions and perpendicular to it is controlled using piezoelectric actuators. The cantilever's deflection is most commonly detected by using the laser beam method. Here, the cantilever's backside, which has a reflective coating, is illuminated with a laser beam which is reflected to a split photodiode. If the cantilever deflection changes, the laser spot on the photodiode moves accordingly. This movement can be measured as the difference of the signals between the upper and lower half of the photodiode and is proportional to the cantilever deflection. From the deflection of the cantilever, the height information at a given point x_i, y_i from the sample surface is recorded. In figure 2.4 the schematic principle of an AFM is illustrated.

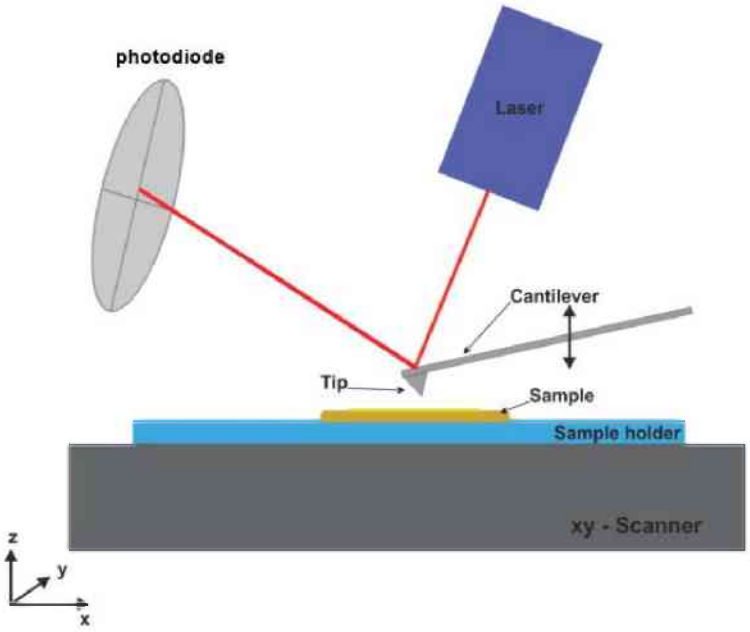

Figure 2.4: Scheme of the AFM principle.

In AFM, a sample's topography can be recorded with three principal modes: contact mode, non-contact mode and tapping mode. In contact mode, the tip is permanently in contact with the sample surface. To obtain a height information, the signal of the cantilever's deflection is used by either keeping the deflection constant and recording the z-piezo movement or keeping the height constant and recording the deflection. The permanent contact between tip and sample can influence or even damage the surface of soft materials. In non-contact mode, the cantilever is oscillating near its resonance frequency away from the surface and never touching it. The damping of the amplitude can be detected and used to adjust the height by movement of the z-piezo. In general, non-contact mode yields higher resolution and has a low likelihood to influence the surface, but is usually only applied in ultra-high vacuum. Tapping mode is a combination of contact and non-contact mode. Here, the cantilever is also oscillating near its resonance frequency but is periodically touching the surface [24]. If the distance between tip and surface decreases, the damping of the oscillation increases leading to a reduction in amplitude. A control loop, however, tries to hold the oscillation amplitude constant by moving the cantilever in z-direction. The movement of the z-piezo is then recorded and represents the sample's topography. In tapping mode, it is possible to record the phase shift signal between the exciting oscillation and the actual oscillation of the cantilever [25]. The phase shift is a measure of the energy dissipation involved in the contact of the tip with the sample, which depends on many properties, including viscoelasticity, adhesion and also contact area between tip and sample. As contact area is strongly dependent on the local topography, the phase image also contains topographic contributions [26].

2.2.1 Force spectroscopy

An AFM force-distance curve is a plot of tip-sample interaction forces vs. tip-sample distance. In order to obtain such a plot, the tip is ramped along the axis perpendicular to the sample surface and the cantilever deflection δ_c is acquired. The tip-sample force F is given by Hooke's law:

$$F = k_c * \delta_c. \qquad 2.1$$

In figure 2.6, an ideal force-distance curve is illustrated. The approach and withdrawal force-displacement curves are both characterized by three regions, the zero line, a discontinuity and the contact line. Along the zero line (position 1 in figure 2.6) the cantilever is in its resting position. Here, the tip is far away from the surface and nearly no forces are exerted. As the tip gets closer to the surface, the interaction between tip and surface increases until the discontinuity (position 2) is reached. This indicates the jump-to-contact (JTC). It means, that the gradient of the tip-sample force is now larger than the elastic constant of the cantilever. The “JTC” point gives information on attractive forces between tip and sample, but has no further meaning for this work. As the contact continues along the contact line (position 3) until a maximum force is reached, the cantilever bends with a positive curvature and repulsive forces increase. At the turning point (position 4) the tip starts to withdraw from the surface until the jump-off-contact (JOC) occurs (position 5) and the cantilever bends with a negative curvature below the zero line. Here, the pull-off force equals the adhesion force (F_{ad}). In figure 2.7, actually measured force-distance curves are presented. The difference in force for JOC is clearly visible and indicates high and low adhesion force.

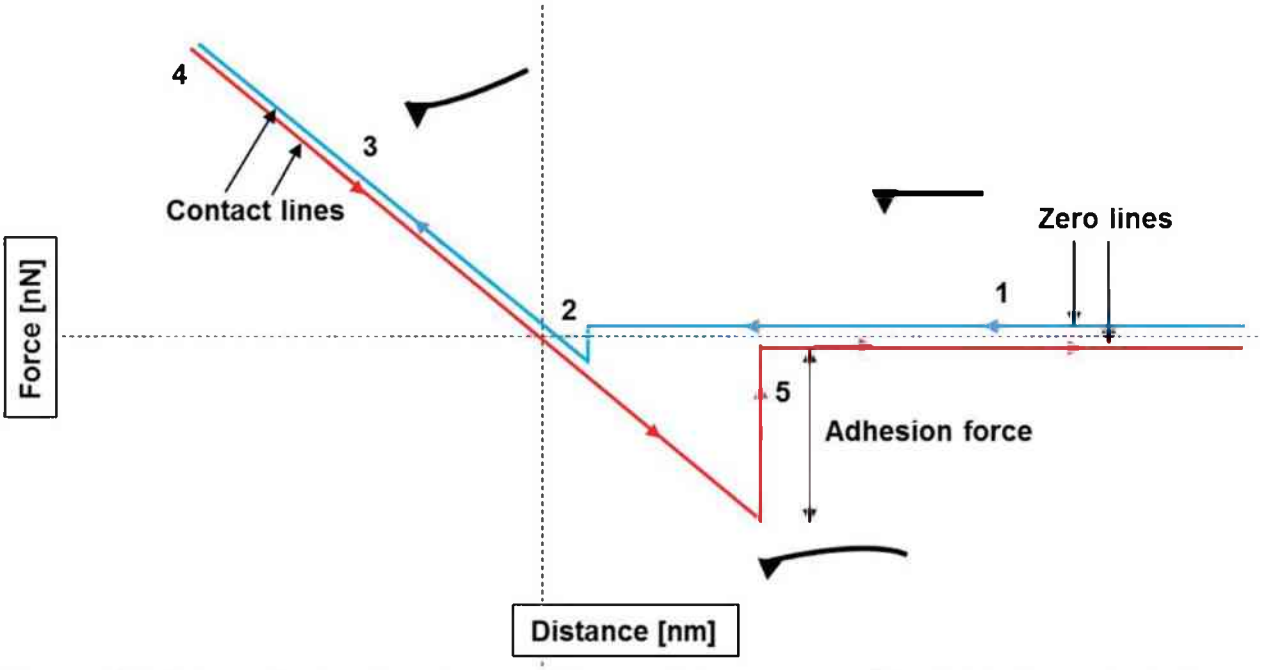

Figure 2.6: Schematic drawing of a model force–distance curve. At point 1, the probe is far from the surface, at 2 "JTC" occurs as attractive forces pull the probe onto the surface. The force becomes repulsive as the probe continues to be driven towards the sample. At the maximum force (4), the direction of travel reverses. At point 5 "JOC" occurs as the force applied to the cantilever overcomes tip–sample adhesion. Also, the cantilever deflection at the most important positions is indicated.

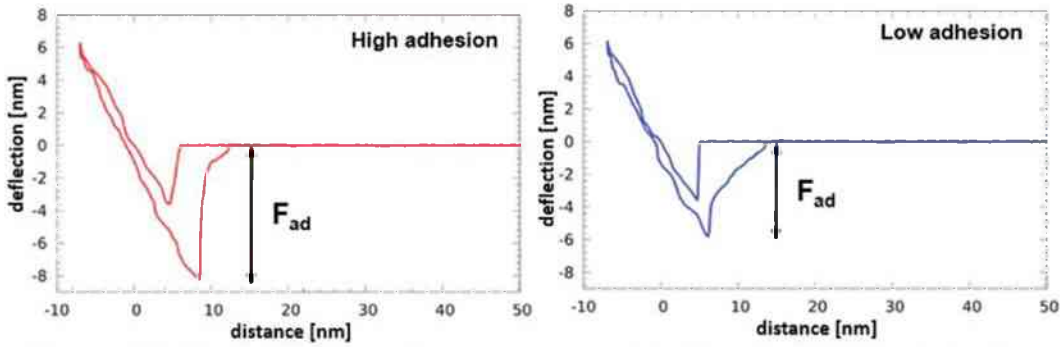

Figure 2.7: Measured force-distance curves with different adhesion behavior.

As can be seen in figure 2.6, the "jump off contact" deflection and distance are always larger than the "jump to contact" deflection and distance. This hysteresis occurs for several reasons. During contact chemical or adhesive bonds may be formed. Also, the sample deforms during contact, which most likely increases the contact area between the tip and sample. Another cause could be capillary forces caused by a water layer on the sample surface, which are adhesive by nature if the tip is hydrophilic. An important factor for measuring force-distance curves is the stiffness of the cantilever used. Especially the discontinuities are dependent on the spring constant k_C of the cantilever. With higher k_C, the JTC increases and the JOC decreases, which also minimizes the hysteresis. If k_C is larger

than the maximum of the tip-sample force gradient, hysteresis and jumps disappear. Though the force resolution is reduced, cantilevers, which are stiff in relation to the sample, should be employed for the measurement of force-distance curves [9].

2.3 Methods for the analysis of AFM images

2.3.1 Roughness analysis

Because of the measurement principle, the recorded AFM image z (x_i, y_i) allows a quantitative analysis of surface roughness. Using the software package Gwyddion [27], the 1D height-height correlation function (HHCF) can be calculated from the recorded topography images. The HHCF C(x) is obtained [22, 23] by the relation

$$C(x) = < [h(x_0 + x) - < h(x) >] * [h(x_0) - < h(x) >] >, \qquad 2.3$$

where x is a point on the surface and h(x) is its height. Equation 2.3 is then fitted with

$$\mathrm{C(x)} = \sigma \cdot \mathrm{e}^{-(\frac{|x|}{\xi})^{2\alpha}}, \qquad 2.4$$

to obtain the root mean square (RMS) roughness σ, the lateral correlation length ξ, and the Hurst parameter α for random rough surfaces with a cut-off [30]. Here, σ describes the standard deviation of the height values and ξ the lateral roughness fluctuations. The Hurst parameter α is a measure for the jaggedness of the surface. An α closer to zero corresponds to a more jagged surface, in contrast an α closer to 1, which describes a smoother surface. In figure 2.8 an example of HHCF and its fit are shown.

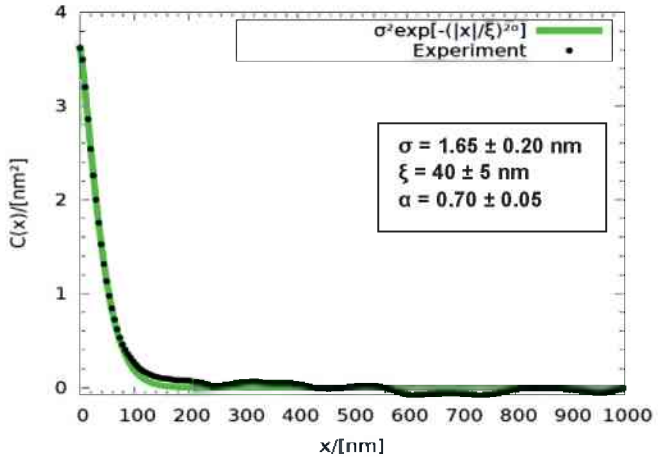

Figure 2.8: 1D HHCF and fit from a 5 x 5 µm² topography measurement of a filtrated cellulose xylan film. Here, σ^2 is given by the maximum of the curve, ξ is at 1/e decay of the curve and α is indicated by the form of the graph.

3 Experimental

3.1 Sample treatment

3.1.1 Xylan powders

The adsorption behavior of two different xylan samples on cellulosic materials was investigated. Both powder samples were provided and characterized via chromatography methods at Lenzing AG. Xylan X_1 was extracted from a beech sulfite dissolving pulp and Xylan X_2 from eucalyptus kraft pulp. The samples differed in molecular weight and chemical composition, as is detailed in table 3.1.

Table 3.1: Molecular weight and chemical composition of the used xylan powders. MeGlcA = methylglucuronic acid, Ara = arabinose, Gal = galactose, Glu = glucose, Man = mannose, Xyl = xylose.

	Molecular weight [kgmol^{-1}]		Chemical composition [%]						
Sample	M_n	M_w	MeGlcA	Ara	Gal	Glu	Man	Xyl	total
X_1	4.6	5.6	4.8	0.1	0.0	0.8	0.4	90.6	96.7
X_2	9.0	17.6	3.7	0.0	0.4	0.2	0.0	89.4	93.9

3.1.2 Cellulose model films

Thin cellulose model films [31] were prepared at Graz University of Technology where also the adsorption was performed by Albrecht Miletzky [14].

Trimethylsilyl cellulose (TMSC) was mixed with toluene and afterwards spin-coated onto quartz crystals. The TMSC films were then transformed into amorphous cellulose by exposure to vapor of 10 wt% HCl-solution. Solutions of 1 g/l xylan X_1 were prepared with varying pH (7, 8 and 9) and ionic strength (1 mmol/l and 100 mmol/l NaCl). The adsorption of xylan was verified by a quartz crystal microbalance (QCM) with dissipation monitoring. First, the sensors were equilibrated with MQ water and a NaCl solution. Then, the xylan solution was pumped over the samples at a flow rate of 0.1 ml/min for 60 min. Afterwards the films were rinsed with a NaCl solution and MQ water for 30 min each. In table 3.2 an overview of all the prepared samples is provided.

Table 3.2: Overview of the samples and the films' variation in pH and ionic strength.

Sample name	pH	Ionic strength
cell_xyl_pH7	7	-
cell_xyl_pH8	8	-
cell_xyl_pH9	9	-
cell_xyl_pH7_1	7	1 mmol NaCl
cell_xyl_pH8_1	8	1 mmol NaCl
cell_xyl_pH9_1	9	1 mmol NaCl
cell_xyl_pH7_100	7	100 mmol NaCl
cell_xyl_pH8_100	8	100 mmol NaCl
cell_xyl_pH9_100	9	100 mmol NaCl

3.1.3 Native cellulose fibers

The native cellulose fiber samples were provided by Mondi Frantschach. The samples were industrial grade kraft pulp fibers in the never dried state [32] (called Monopol by Mondi which is a mixture of spruce and pine fibers). Further treatment was done at Graz University of Technology by Albrecht Miletzky [14].

Xylan powder was dissolved in 1 mol/l sodium hydroxide (NaOH). During stirring (X_1 for 15 min, X_2 for 25 min) it was heated to 55°C for dissolution and cooled down afterwards. The pulp was heated and mixed with deionized water, with the addition of NaCl to separate the fibers. Then the xylan solution was added to this suspension at 80°C. For xylan precipitation on the fiber surface, the pH was adjusted to 7 with H_2SO_4.

During the adsorption, the xylan concentration varied between 80 mg/g and 320 mg/g.

Table 3.3: Overview of kraft pulp fiber samples and xylan characteristics.

Sample name	xylan powder	xylan content [mgg^{-1}]
MXB_ref	-	-
MXB_X1_80	X_1	80
MXB_X2_80	X_2	80
MXB_X1_320	X_1	320
MXB_X2_320	X_2	320

3.2 Sample preparation

3.2.1 Cellulose model films

For the cellulose model film samples, no further preparation was required. As described above, cellulose films were deposited on QCM sensors and are presented in figure 3.1.

Figure 3.1: Photography of cellulose model films on QCM sensors.

3.2.2 Native cellulose fibers

A small piece of a silicon wafer was randomly scratched as an orientation aid and glued to a round steel sample holder with nail polish [33]. Then, the fiber was placed on the silicon and fixed at both endings using also nail polish, as illustrated in figure 3.2.

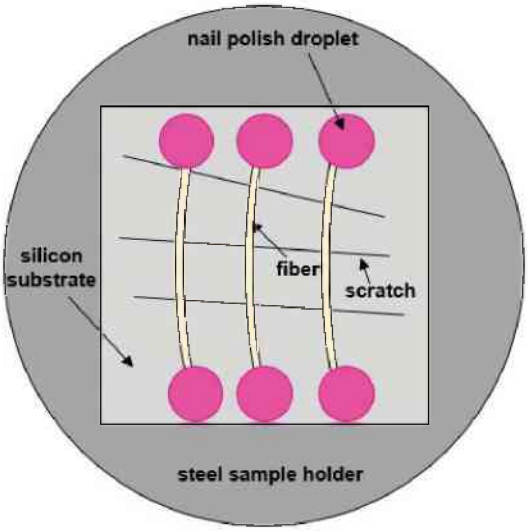

Figure 3.2: Principle of a prepared fiber.

3.3 AFM Setup

An Asylum Research MFP 3D AFM, presented in figure 3.3, was used for all measurements in this work. The instrument is equipped with a planar closed loop scanner, so the actual movement of the piezoelectric actuator is monitored by an inductive sensor. Due to this setup, an online correction of the expansion or contraction of the piezoelectric actuators by a feedback loop is achieved.

Figure 3.3: Photograph of an Asylum Research MFP 3D AFM.

3.3.1 Phase imaging

The phase shift between excitation and the detected oscillation of the cantilever in tapping mode provides a material contrast. This material contrast is caused by a difference in viscoelastic properties of the sample, resulting in a difference in energy dissipation and, therefore, phase shift [28, 29]. In figure 3.4 the method is depicted schematically.

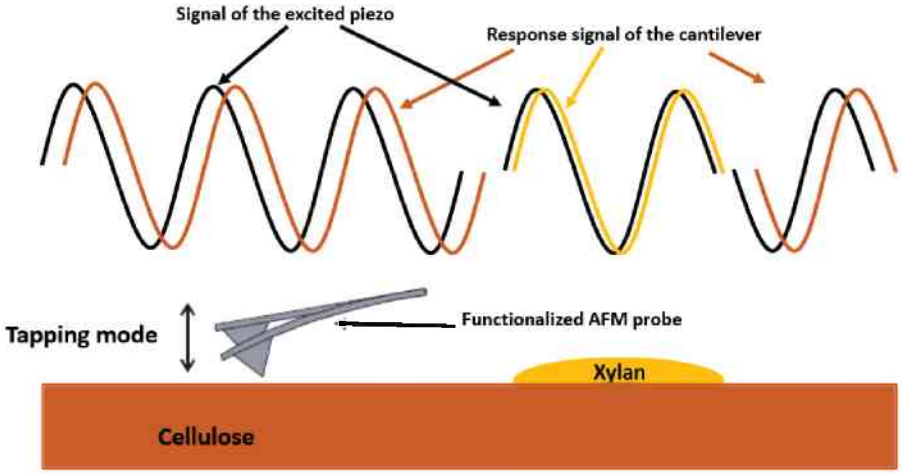

Figure 3.4: Principle of phase imaging.

3.3.2 Force mapping

In figure 3.5, the principle of force mapping [36] is illustrated. For all the measurements in this work, force maps of 64 x 64 pixels were recorded. A force distance curve was measured for each pixel and a pixel's color represents the magnitude of the adhesion force at this point. The adhesion force F_{ad} is the minimal point of the withdrawal curve (blue line in figure 3.5).

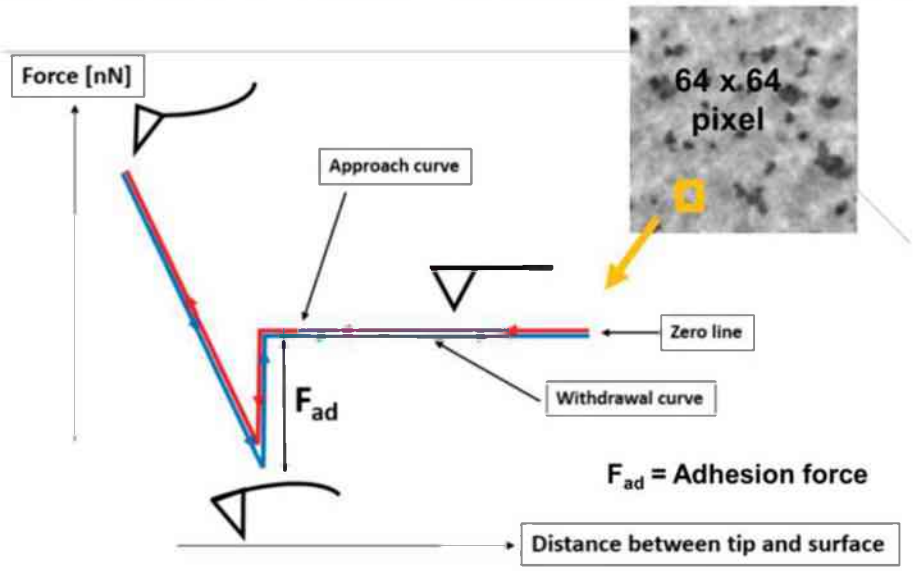

Figure 3.5: Principle of force mapping.

Before each measurement, the cantilever's spring constant was calibrated. This was performed by Asylum Research's "GetReal" calibration procedure [37], which utilized the thermal sweep method [38] in combination with Sader's method [39]. For this method, only the cantilever geometry and its first resonance frequency is needed as an external input. Then the algorithm measures the thermal noise spectrum automatically and calibrates the spring constant k and the inverse optical lever sensitivity InvOLS [40].

Compared to the conventional method, the "GetReal" feature has the advantage that the risk of damaging the tip is reduced, because a force curve on a hard surface to calibrate InvOLS is not needed anymore.

3.4 AFM Probes

For topography measurements on the cellulose films in tapping mode, Olympus AC240TS probes were used. Due to their low spring constant, they are suitable for softer materials, details are shown in table 3.4 and 3.5. For the rougher paper fibers, the topography was measured with Olympus AC160TS probes, details are also listed in table 3.4 and 3.5.

Table 3.4: Tip specifications of the used probes. (For Olympus probes from [41].)

probe	material	shape	radius [nm]	height [µm]	front angle [°]	back angle [°]	side angle [°]
AC240TS	Si	3-sided	9 ± 2	14 ± 4	0 ± 1	35 ± 1	15 ± 1
AC160TS	Si	3-sided	9 ± 2	14 ± 4	0 ± 1	35 ± 1	15 ± 1
modified probes	Si	-	40 ± 20	-	-	-	-

AFM probes with functional groups attached at the tip are commercially available (NanoCraft coating GmbH, Engen, Germany) and were used in this work for phase imaging and force mapping to get a chemical contrast [42]. The probes were modified with hydrophilic OH- or hydrophobic CH_3-groups, as indicated in figure 3.6. The producer provided only data of the cantilevers, which is listed in table 3.5.

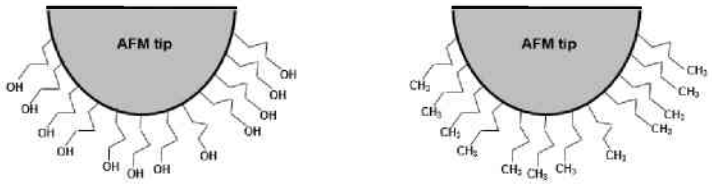

Figure 3.6: Illustration of modified OH- and CH_3- tips

Table 3.5: Cantilever specifications of the used probes. (For Olympus probes from [10].)

probe	material	resonance [kHz]	spring [Nm^{-1}]	length [µm]	width [µm]	thickness [µm]
AC240TS	Si	50 - 90	0.5 - 4.4	230 - 250	28 - 32	1.7 - 3.7
AC160TS	Si	200 - 400	12 - 103	150 - 170	48 - 52	3.6 - 5.6
OH-modified	Si	160	7	150	27	2.8
CH3-modified	Si	160	7	150	27	2.8

For the estimation of the tip radius a commercially available TGT01 calibration grid (NT-MDT, Moscow, Russia) was used before measurements. There, spikes with an opening angle of 30° and a tip radius of 10 nm are arranged periodically. In figure 3.7, an OH modified tip and its height profile at the indicated position are presented. The value for the tip radius of the modified probes presented in table 3.4 is the average of the distance measurements in five different height profiles.

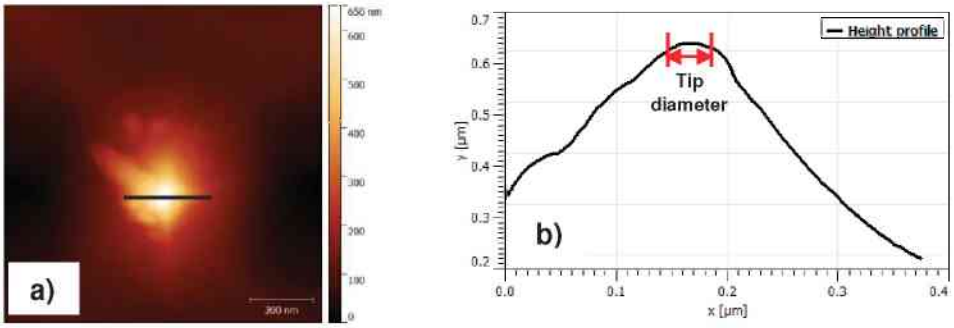

Figure 3.7: In image a) a height image of an OH modified tip is shown. The black line indicates the position of the height profile provided in b). It is a cross section of the tip and with the red lines in b) the tip diameter is roughly measured.

4 Results

4.1 Filtrated/unfiltrated cellulose/xylan films

4.1.1 Roughness analysis

AFM measurements were performed to investigate the morphology and evaluate the roughness of cellulose model films with adsorbed xylan. For two of the four films, a "ChromaFil" 0.45 µm filter was used during sample preparation to check the effectiveness of the filter [43].

Figure 4.1 shows 5 x 5 µm² AFM scans of the surface topography of all four samples. In figure 4.2 more detailed 1 x 1 µm² topography images of the samples are depicted.

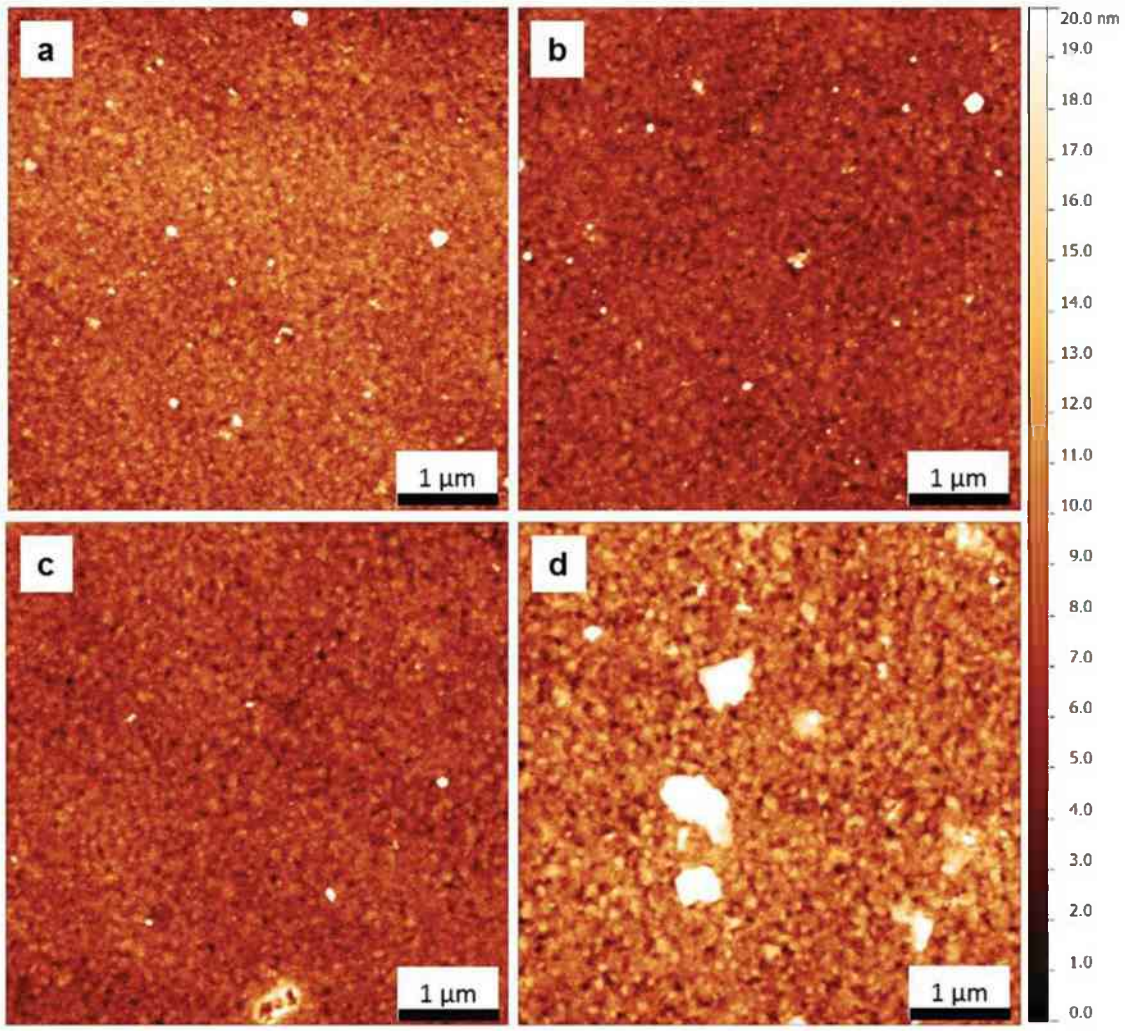

Figure 4.1: 5 x 5 µm² topography scans of the (a), (b) filtrated, and (c), (d) unfiltrated samples.

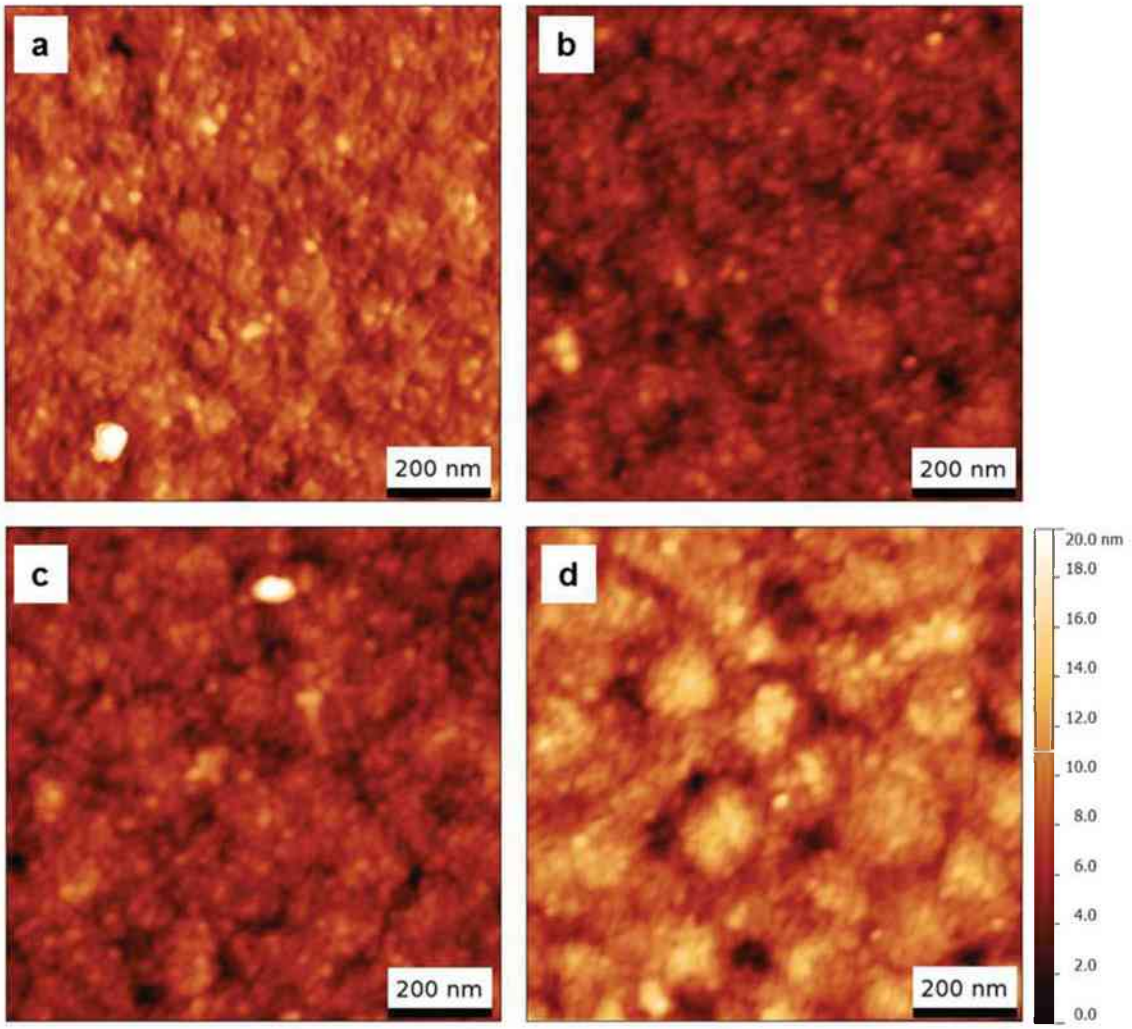

Figure 4.2: 1 x 1 µm² topography scans of the (a), (b) filtrated and (c), (d) unfiltrated samples.

In the 5 x 5 µm² topography scans of the unfiltrated #2 sample, large aggregates on the surface – about 0.4 µm – 0.5 µm in lateral dimensions and 20 nm - 30 nm in height - are visible (see figure 4.1). On the corresponding 1 x 1 µm² images, the hill-like surface structure seems more enhanced than in the other samples' images (compare figure 4.2). Additionally, surface features with a lateral size of about 30 nm – 40 nm, are observed for all samples and do not differ significantly for the filtrated and unfiltrated sample. The lateral dimensions were measured by line profiles.

In table 4.1 the results of the roughness analysis for the 5 x 5 µm² and the 1 x 1 µm² topography scans are presented. The values in the table are given as average and standard deviation of 3 independent positions from one sample. The calculation of the main three parameters, RMS roughness σ, lateral correlation length ξ and Hurst parameter α, has been described in detail in chapter 1.

Table 4.1: Results of the roughness analysis for the filtrated/unfiltrated films. The values for rms roughness σ, lateral correlation length ξ and roughness parameter α are given as average and standard deviation from 3 independent positions on the sample surface.

	5 x 5 µm²			1 x 1 µm²		
	σ [nm]	ξ [nm]	α	σ [nm]	ξ [nm]	α
Filtrated						
#1	1.65 ± 0.20	40 ± 5	0.70 ± 0.05	1.50 ± 0.15	30 ± 5	0.70 ± 0.05
#2	1.55 ± 0.15	40 ± 5	0.70 ± 0.05	1.30 ± 0.05	30 ± 5	0.75 ± 0.05
Unfiltrated						
#1	1.75 ± 0.30	60 ± 10	0.65 ± 0.05	1.40 ± 0.15	30 ± 5	0.70 ± 0.05
#2	3.25 ± 0.70	110 ± 50	0.65 ± 0.20	2.15 ± 0.15	40 ± 5	0.85 ± 0.05

The RMS roughness σ is similar for most samples, only the unfiltrated #2 sample shows a higher σ. This could explain the difference in RMS roughness σ. A similar trend is observed for the lateral correlation length ξ. Only for the 5 x 5 µm² topography images of the unfiltrated #2 sample, a significantly higher ξ is found. Otherwise ξ and also the Hurst parameter α do not show any differences.

4.1.2 Phase imaging

To provide a chemical contrast between xylan and cellulose, OH-functionalized tips were employed for imaging. If such tips can detect the differences between cellulose and xylan, it should lead to a contrast in the recorded phase images. The method is described in more detail in chapter 3. In theory, xylan should be more hydrophilic [44] and has a stronger interaction with the hydrophilic OH-groups. In figure 4.3, exemplary topography and phase images of the filtrated samples are provided. The method was only performed on the filtrated samples because the roughness analysis already showed no significant difference between the filtrated and unfiltrated samples.

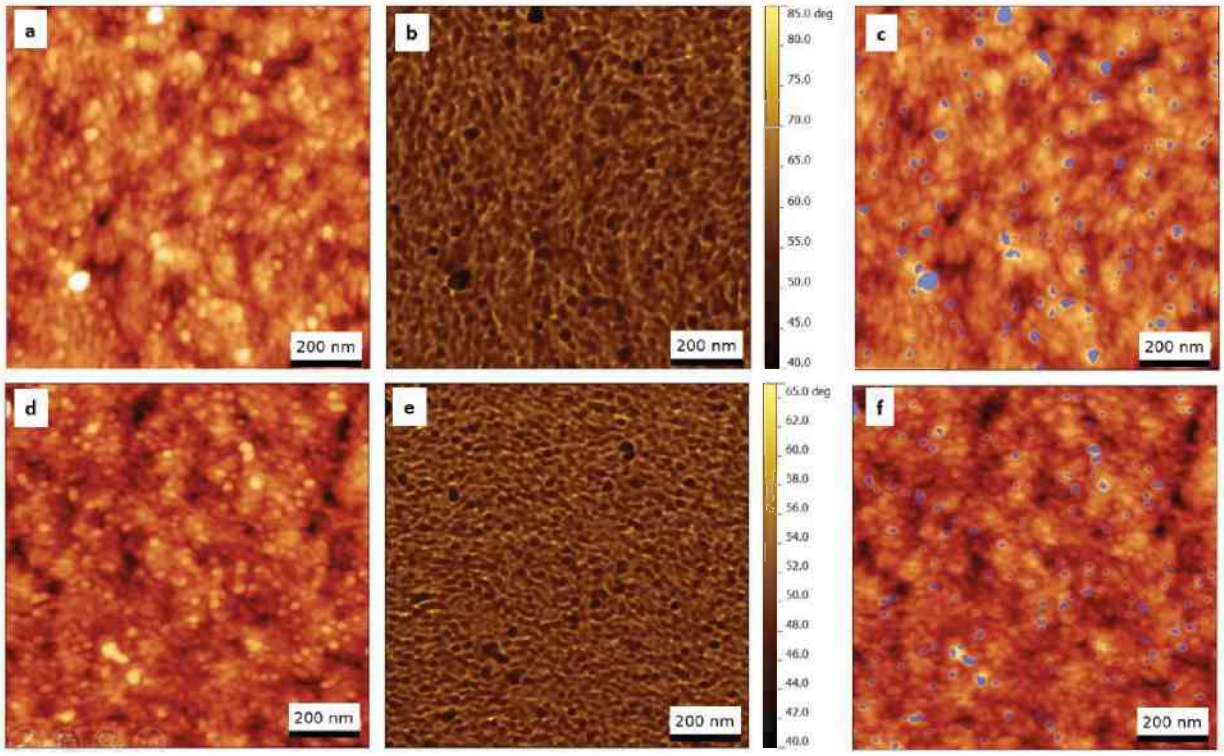

Figure 4.3: Exemplary topography (a), (d) (z-scale: 15 nm), and phase (b), (e) images of the filtrated samples recorded with an OH-functionalized tip. In (d) and (f), regions with a low phase shift which is dark in the phase images are marked in blue.

At first, it seems that there can be a contrast detected [45]. With the Gwyddion [27] software package it was possible to mark regions with low values in the phase images and put these masks on the corresponding topography images. Such marked topography images are presented in figure 4.3c and f. The masked topography images for both samples show that only small, mostly spherical features with a diameter of about 10 nm – 15 nm and a height of about 5 nm – 10 nm lead to a phase contrast. The rest of the phase images looks rather uniform. However, it is not possible to definitely correlate the obtained contrast with differences in chemical composition of the sample. Since all regions with low phase are found on elevated, steep sloped structures, one has to assume that a topographical influence is more likely than the expected chemical difference for the phase contrast.

In order to investigate this phenomenon in detail also a model film with pure cellulose was prepared. Figure 4.4a shows topography and phase contrast of the pure cellulose film. In figure 4.4b, the topography and phase image for an exemplary cellulose/xylan film is presented. A comparison between the phase images of a pure cellulose film and one of a cellulose/xylan film, as in figure 4.4a and b, shows a difference in phase contrast. Particularly, the phase image of the cellulose film (phase: 60.20° ± 2.00°) is slightly more uniform than the cellulose/xylan film (phase: 57.90° ± 3.80°). Moreover, this effect can also be explained by the difference in the samples topographies.

The pure cellulose film (σ = 0.65 nm) is smoother than the cellulose/xylan film (σ = 1.55 nm). This should be the reason for the deviation in the mean phase value.

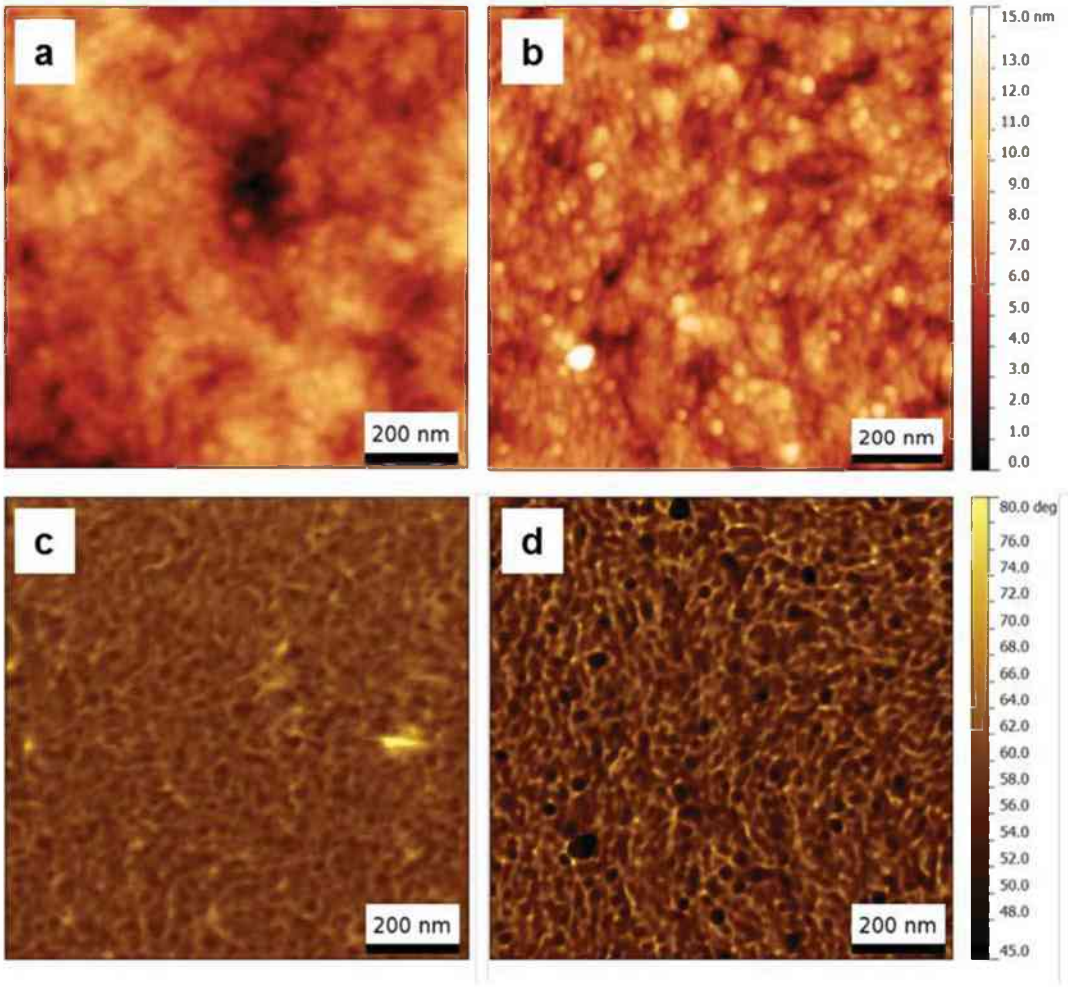

Figure 4.4: Topography and corresponding phase images of (a), (c) a pure cellulose film and (b), (d) a cellulose/xylan film.

4.1.3 Force mapping

Another way to obtain a chemical contrast is AFM adhesion force mapping with OH-functionalized tips. See chapter 3 for a detailed description of this method. In comparison to phase imaging, the probe does not operate in tapping mode, but force-distance curves are recorded. The adhesion force is measured when the tip is pulled off the surface. A 64 x 64 pixel (px) map with the adhesion values of each individual force-distance curve is provided at the end of the measurement.

The applied maximum force during these measurements was kept at about 20 nN to ensure only elastic deformations of the films. The recording of the force distance curves was started 500 nm above the sample's surface, and the curves were acquired with a rate of 2 Hz for all measurements. With every new measurement and every new tip, the probe's spring constant

had to be calibrated according to [37], as described in chapter 3.3.2 to choose the right trigger point which sets the applied force.

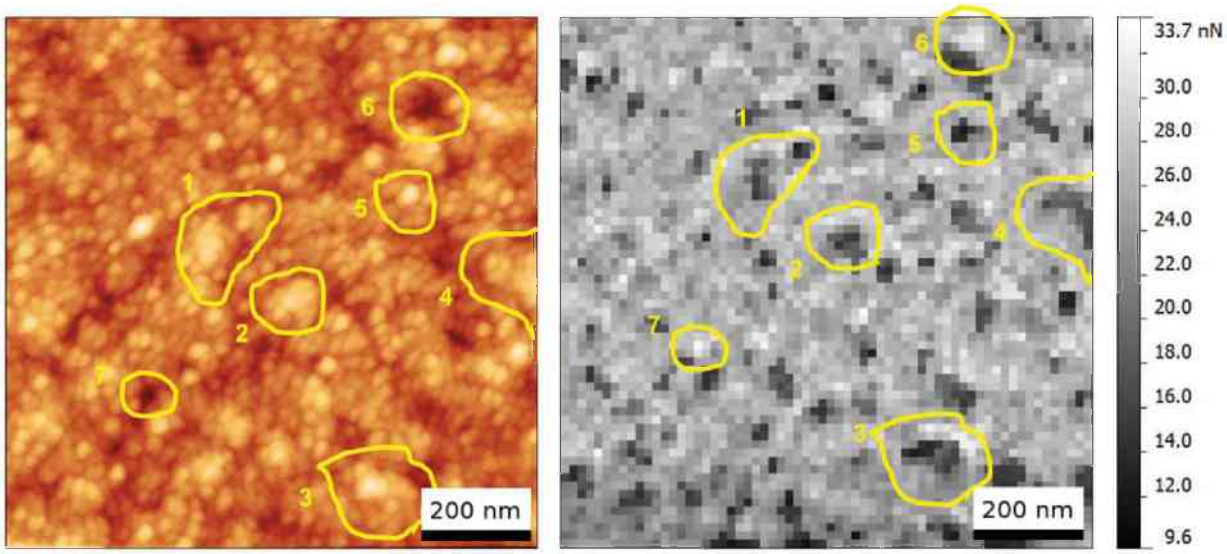

Figure 4.5: 1 x 1 µm² topography (z-scale: 15 nm) and 64 x 64 px adhesion force maps with OH-functionalized probes of one of the filtrated samples. The yellow marked regions show corresponding areas.

In figure 4.5, the 1 x 1 µm² topography and adhesion images of the filtrated sample are shown. In the adhesion image, a contrast is visible. The yellow marked regions indicate exemplary corresponding areas. The marked areas are slightly shifted. This is due to thermal drift, because the topography image was recorded first and took about five minutes, but the force map takes more than half an hour. Area 1-5 in figure 4.5 show a lower adhesion force and correspond to a higher position in the topography image, whereas area 6 and 7 show a slightly higher adhesion and correspond to a more pit-like surface location. This represents, similar to phase imaging, a topographical effect.

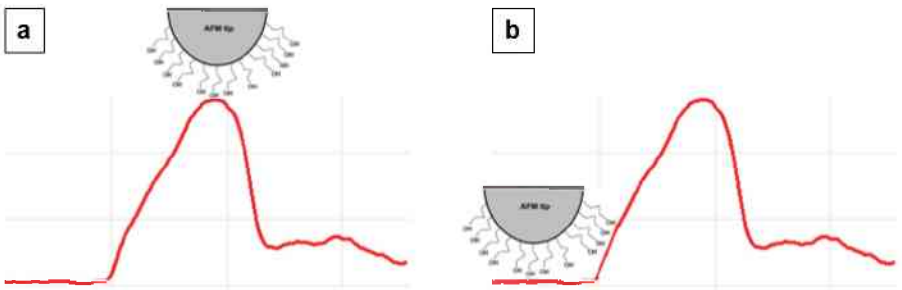

Figure 4.6: Illustration of the modified tip moving (a) on top of a surface hill and (b) in a pit-like region.

This effect is schematically illustrated in figure 4.6. It indicates the movement of the functionalized tip along the surface. Due to the fact that the surface has a certain roughness and is not completely smooth, there are zones where the contact area of the tip with the surface is either lower or larger. Since the adhesion force is proportional to the contact area, an influence to the adhesion force is expected. Figure 4.6a shows the tip on top of a surface hill, here it has less contact which leads to a lower adhesion. If the tip is in a pit or valley, there is more contact area, as shown in figure 4.6b, and also the adhesion is higher.
500 x 500 nm² topography and adhesion scans of the same sample are provided.
In figure 4.7, with the higher lateral resolution of the force maps, the aforementioned topographical effect is even more pronounced. Protrusions correspond to lower adhesion and at pit positions the adhesion is higher.

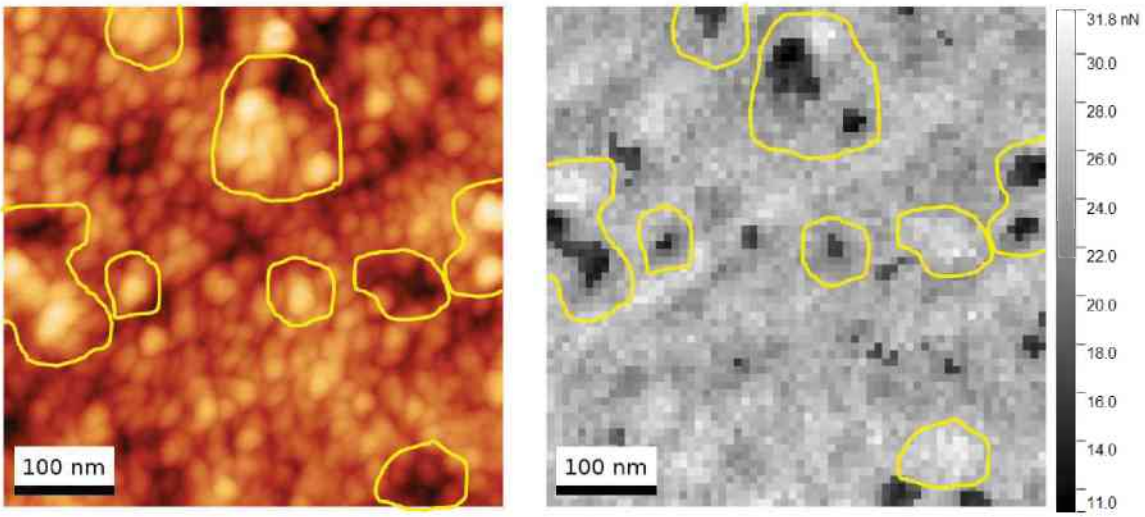

Figure 4.7: 500 x 500 nm² topography (z-scale: 15 nm) and 64 x 64 px adhesion force images of one of the filtrated samples. The yellow marked regions indicate corresponding areas.

4.1.4 Summary

In the topography measurements, almost no differences between filtrated and unfiltrated were found. Only the unfiltrated #2 sample has a higher σ. The filter probably removes these larger particles which are found on the unfiltrated #2 sample.
Phase contrast is seen between protrusions and background. Here, the protrusions have a lower phase shift. It is not clear if the phase images are influenced by topography, but it is most likely.
The detailed force maps with OH-functionalized probes only show topography influence due to non-uniform contact area, a chemical contrast cannot be confirmed.

4.2 Influence of pH and NaCl concentration to xylan adsorption on cellulose

4.2.1 Roughness analysis

AFM topography measurements were performed to determine the surface morphology of nine samples with xylan adsorbed on cellulose surfaces from varying pH (7-9) and NaCl concentration (0, 1 mmol, 100 mmol). In table 4.2 an overview of the different samples and the determined roughness parameters of the roughness analysis are summarized. Figure 4.8-10 show 1 x 1 µm² topography images of all samples.

Table 4.2: Results of the roughness analysis for the cellulose/xylan films. The values are given as averages and standard deviation from 3 independent scans for each sample.

1 x 1 µm²	σ[nm]	ξ [nm]	α [-]
pH=7	2.25 ± 0.30	40 ± 1	0.90 ± 0.05
pH=8	3.70 ± 0.10	45 ± 2	0.80 ± 0.05
pH=9	3.40 ± 0.05	45 ± 5	0.85 ± 0.05
pH=7/ 1 mmol NaCl	2.70 ± 0.10	40 ± 5	0.85 ± 0.05
pH=8/ 1 mmol NaCl	3.50 ± 0.15	50 ± 5	0.90 ± 0.05
pH=9/ 1 mmol NaCl	1.60 ± 0.10	30 ± 5	0.95 ± 0.05
pH=7/ 100 mmol NaCl	2.10 ± 0.15	35 ± 2	0.85 ± 0.05
pH=8/ 100 mmol NaCl	1.90 ± 0.15	35 ± 1	0.90 ± 0.05
pH=9/ 100 mmol NaCl	4.90 ± 1.20	75 ± 20	0.75 ± 0.10

While there are larger, balled features visible for pH=7, the pH=8 sample shows more elongated structures and for pH 9 a dot-like structure is observed. Surface structure sizes analyzed by line profiles will be provided later on.

By comparing the samples prepared without additional NaCl, the highest RMS roughness is found for those with pH=8 and 9. The ξ-values are similar, ranging from 40 – 45 nm. Shape and dimensions of the aggregates on the surface differ with pH.

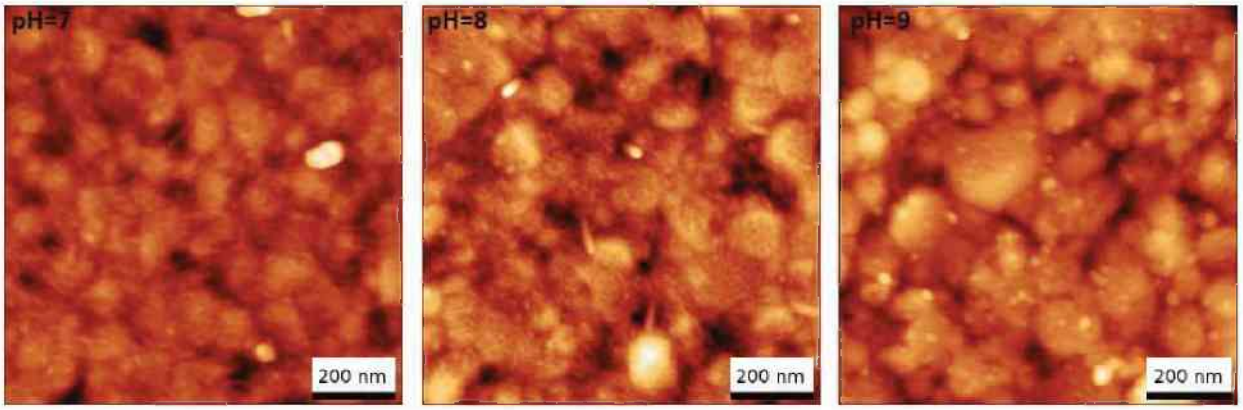

Figure 4.8: 1 x 1 µm² topography images of the samples pH=7, 8 and 9, all without NaCl concentration, z-scale: 30 nm.

For the films with 1 mmol NaCl concentration, shown in figure 4.9, the form of the surface aggregates again shows a similar dependence of pH. On the surface of the samples with pH 7 and 9, small dot-like structures are randomly distributed, whereas the pH 8 sample shows elongated structures.
Here, the sample with pH 8 shows the highest RMS roughness σ and lateral correlation length ξ.

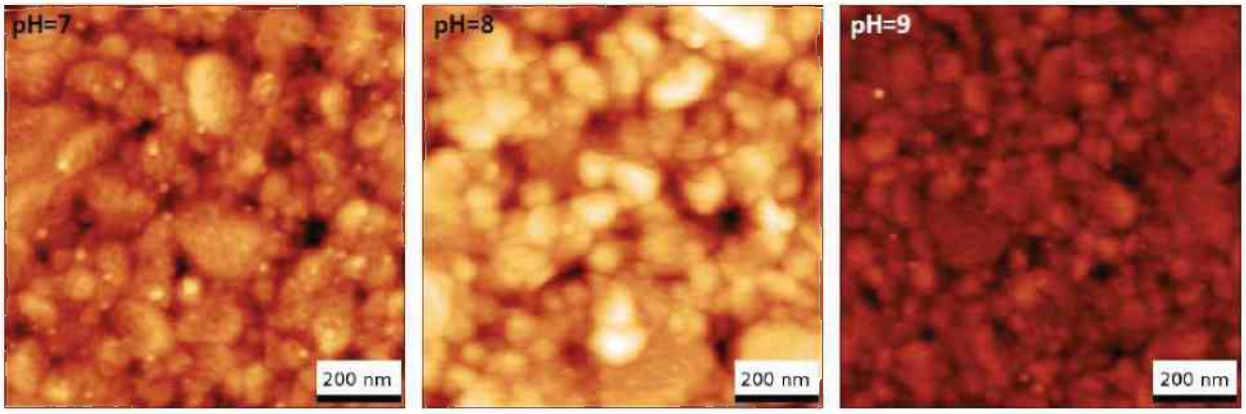

Figure 4.9: 1 x 1 µm² topography images of the samples pH 7, 8 and 9, all with 1 mmol NaCl, z-scale: 25 nm.

The 100 mmol samples, which are presented in figure 4.10, show dot-like aggregates on the surface for all pH values.
The samples with xylan adsorbed from a 100 mmol NaCl solution exhibit similar roughness parameters for pH=7 and 8. The fact that the pH=9 sample is dominated by trenches – additionally to the hill-like structures – is reflected in strongly differing roughness parameters (see Table 4.2).

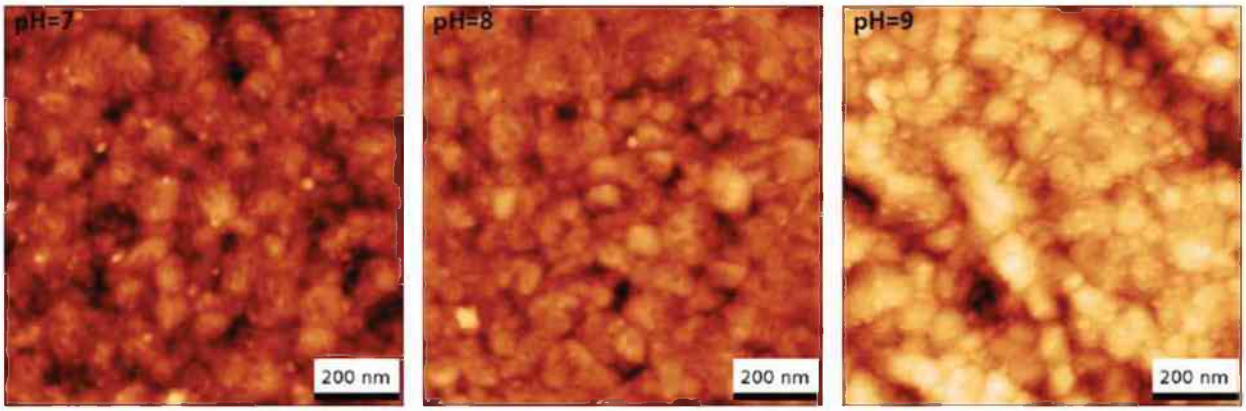

Figure 4.10: 1 x 1 µm² topography images of the samples pH=7, 8 and 9, all with 100 mmol NaCl, z-scale: 25 nm.

σ varies for different NaCl concentrations and different pH. The ξ-values show no real difference for the different pH- and NaCl-variations except for the pH=9/100 mmol sample which shows a larger ξ but also a higher deviation. α behaves similar, again only the pH=9/100 mmol sample shows a smaller Hurst parameter. Figure 4.11 shows a diagram of the σ-pH dependence for all NaCl concentrations. Without NaCl, the RMS roughness increases from pH 7 to 8, and only slightly decreases at pH=9. For 1 mmol NaCl, σ also increases from pH 7 to 8, but decreases quite significantly for pH=9. For the 100 mmol samples, the relation between σ and pH is inverse to the 1 mmol samples. For pH=7 and 8 the films are the smoothest, but for pH=9 the film is the roughest. This is due to the distortion of the surface, which could be a property of the initial cellulose film, before the adsorption of xylan.

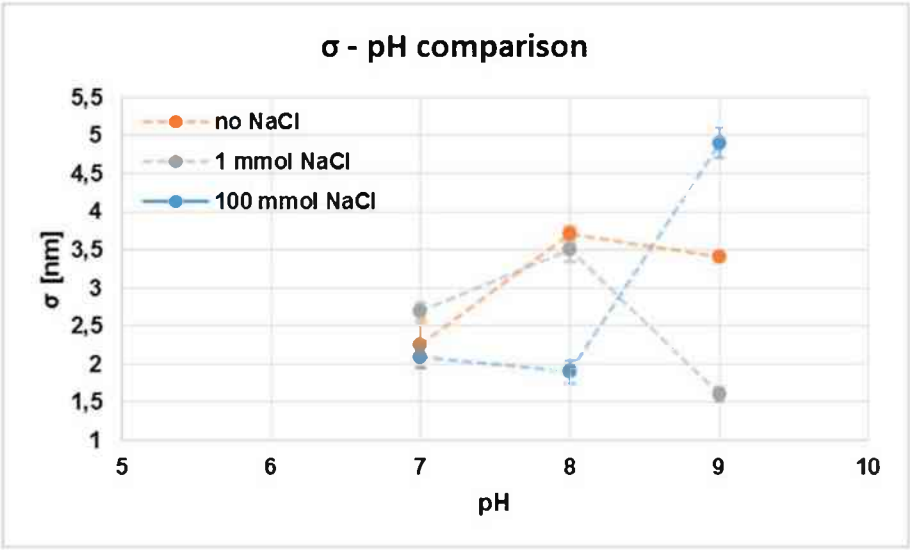

Figure 4.11: Diagram of the σ-pH dependence for all the NaCl concentrations investigated.

To get information on the geometry and size of the surface aggregates, line profiles from one representing topography image of each sample without NaCl were extracted. These are shown in figure 4.12-14 for all 3 pH-variations. In the diagrams of the line profiles, the manually measured dimensions of the aggregates are presented. For every sample, the values for width, height and length were averaged over seven independent line profiles.

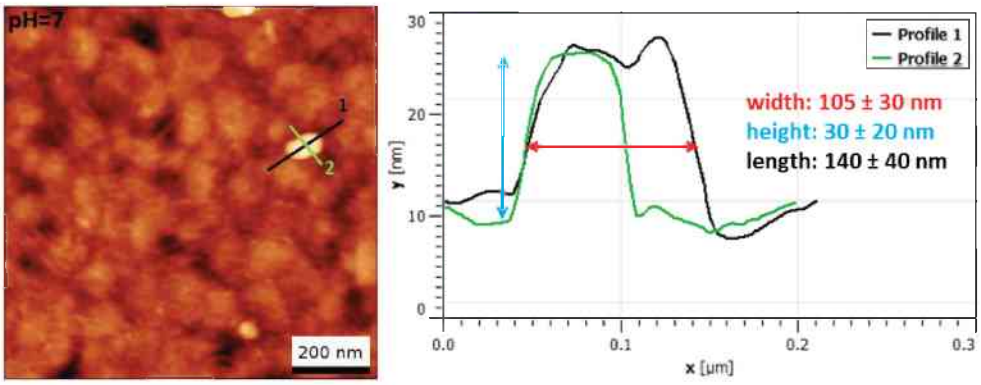

Figure 4.12: a) topography image for the pH=7 sample with position of the line profiles presented in b). The values for width, height and length are also indicated in the line profile. The bars in the line profile indicate the manual measurement.

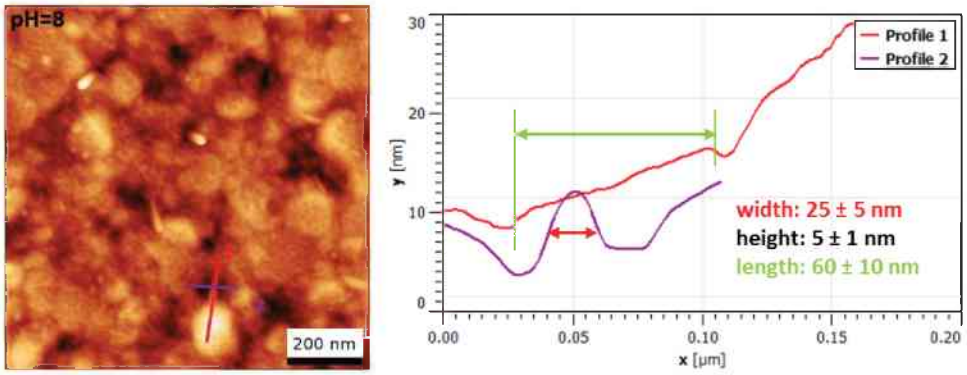

Figure 4.13: a) topography image for the pH=8 sample with position of the line profiles presented in b). The values for width, height and length are also indicated in the line profile. The bars in the line profile indicate the manual measurement.

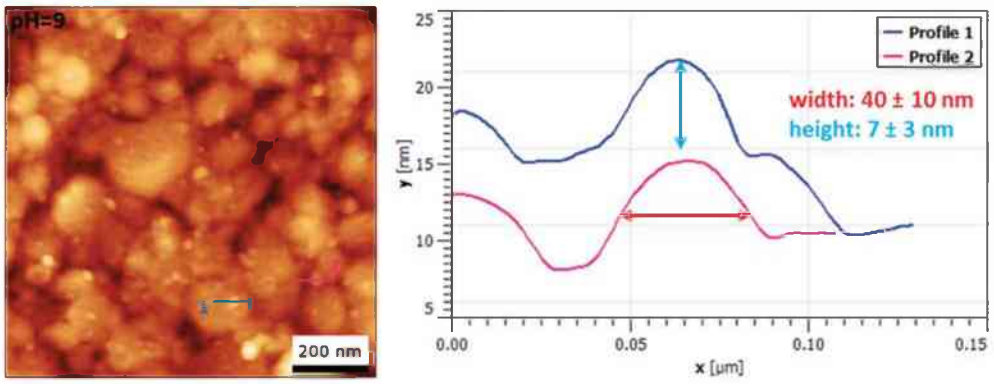

Figure 4.14: a) topography image for the pH=9 sample with position of the line profiles presented in b). The values for width, height and length are also indicated in the line profile. The bars in the line profile indicate the manual measurement.

The topography images already show that the surface structures are either elongated, spherical or dot-like. The elongated features were observed for pH=8/ 0 mmol NaCl and pH=8/ 1 mmol NaCl. The pH=7/ 0 mmol NaCl film shows balled features. For all the other samples, the surface is dominated by a dot-like structure, which is already known from the previously investigated samples of the filtrated/unfiltrated cellulose/xylan films. The dots have a diameter of about (40 ± 10) nm and a height of (7 ± 3) nm. The balled features are in comparison more than twice in diameter with (105 ± 30) nm and approximately three times higher, with a height of (30 ± 20) nm. The elongated structures are much narrower with a width of (25 ± 5) nm and a length of (60 ± 10) nm. In height, these features are very similar to the dot-like structure with (5 ± 1) nm.

Another peculiarity of the elongated structures is that they are located along the slope of the hills. In comparison, the other structures prefer to adsorb mostly on top of the hill-like structure. This is illustrated in figure 4.15.

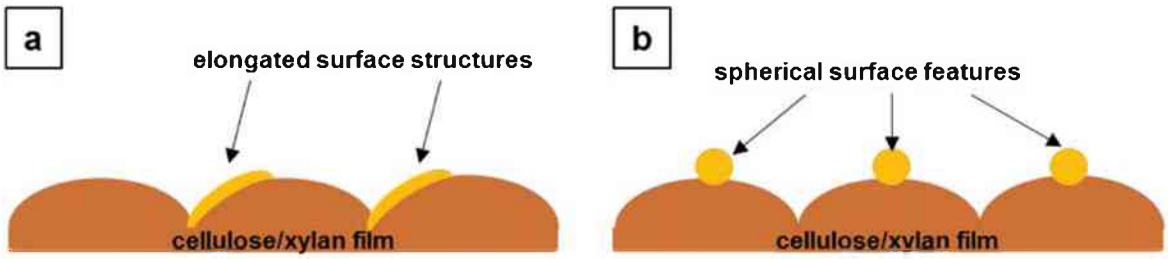

Figure 4.15: Illustration of the position of the a) elongated and b) spherical surface structures.

4.2.2 Phase imaging

Since the investigations of the samples described in 4.1 were not conclusive with OH-functionalized tips alone, here CH_3-functionalized tips were used in addition. In contrast to OH-tips, CH_3-tips are hydrophobic, and a different contrast is expected, if the measured phase is caused only by chemical differences, and not by topography.
In figure 4.16-18 the 1 x 1 µm² topography and phase images were recorded with OH-functionalized tips for all samples.

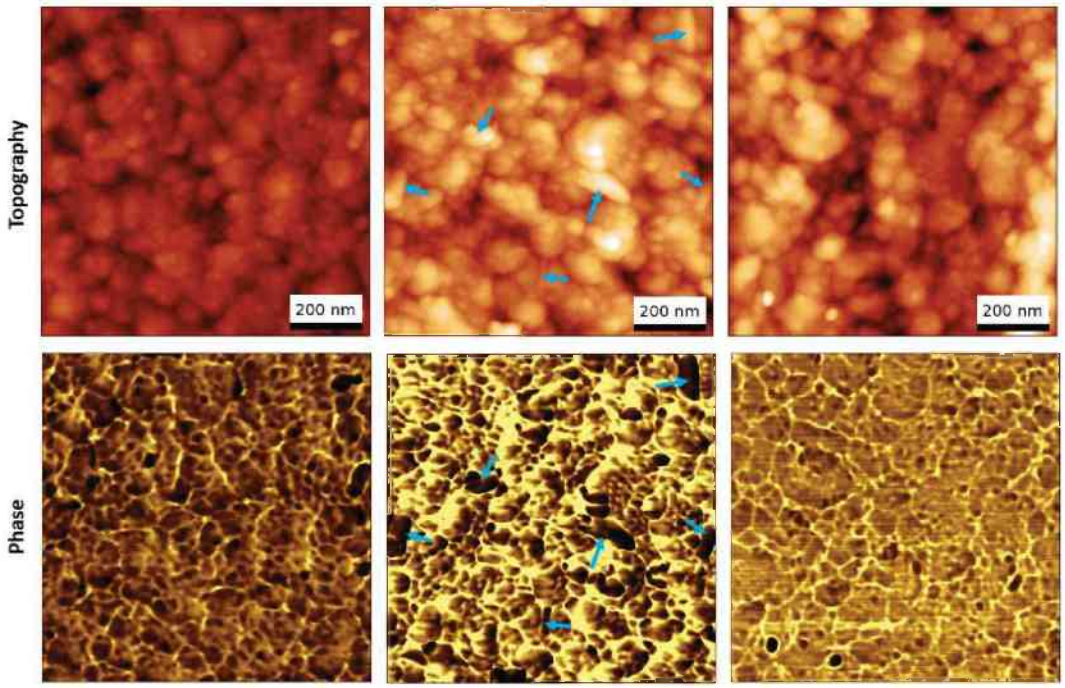

Figure 4.16: 1 x 1 µm² topography (z-scale: 30 nm) and phase images (z-scale: 15°) of the samples pH=7, 8 and 9, all without NaCl, recorded with OH-functionalized tips. The blue arrows in the images of pH=8 indicate areas with stronger phase contrast.

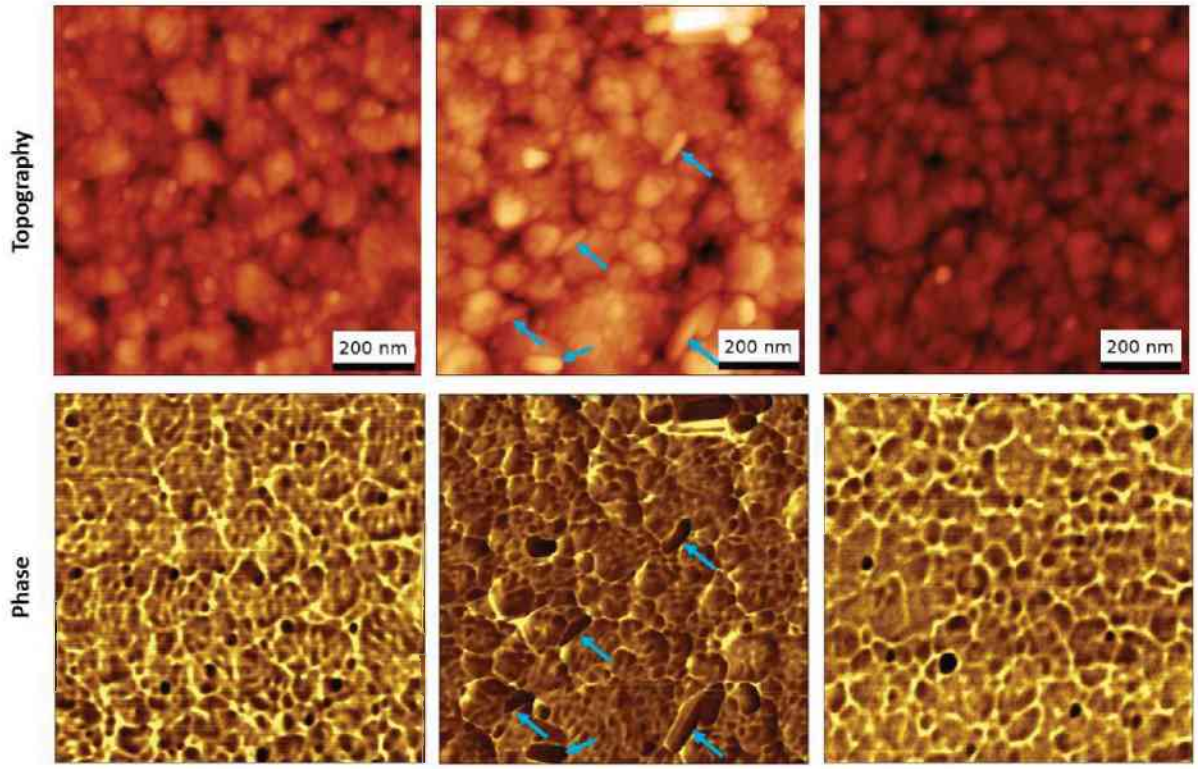

Figure 4.17: 1 x 1 µm² topography (z-scale: 30 nm) and phase (z-scale: 15°) images of the pH=7, 8 and 9 samples, all with 1 mmol NaCl, recorded with OH-functionalized tips. The blue arrows in the images of pH=8 indicate areas with stronger phase contrast.

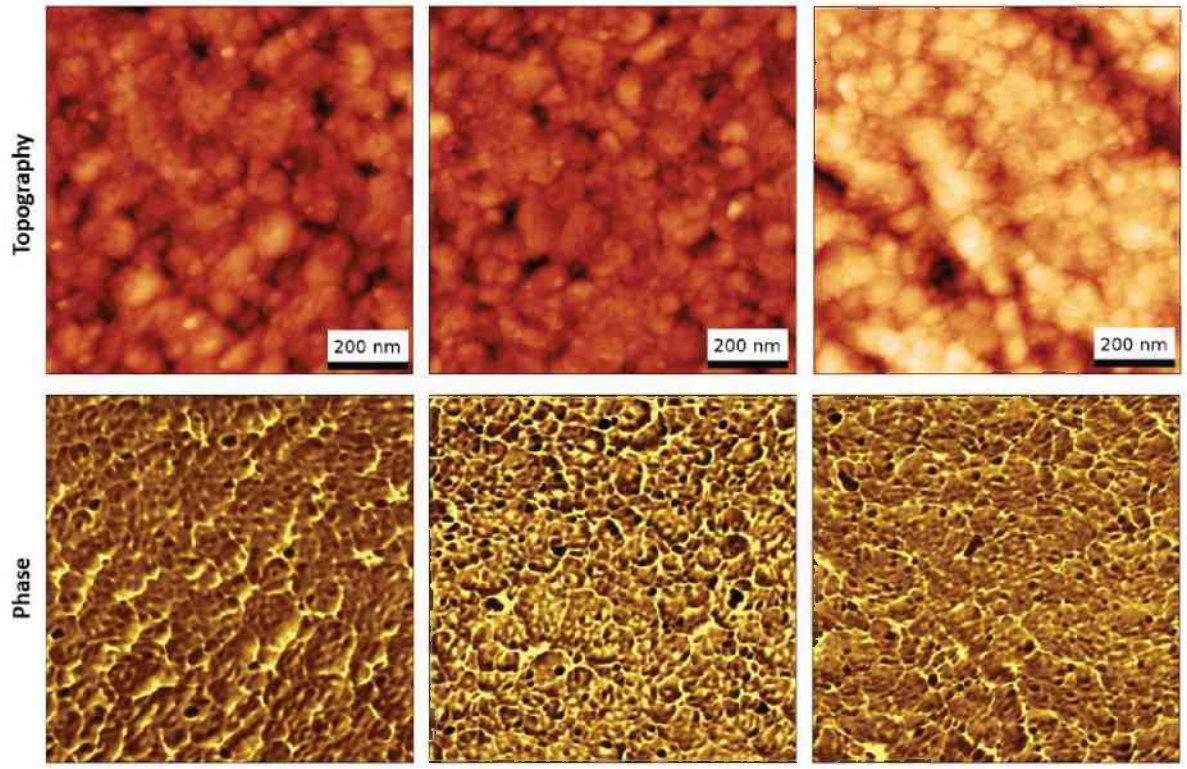

Figure 4.18: 1 x 1 µm² topography (z-scale: 25 nm) and phase (z-scale: 15°) images of the pH=7, 8 and 9 samples, all with 100 mmol NaCl, recorded with OH-functionalized tips.

In figure 4.19-21 the 1 x 1 µm² topography and phase images were recorded with CH_3-functionalized tips for all samples.

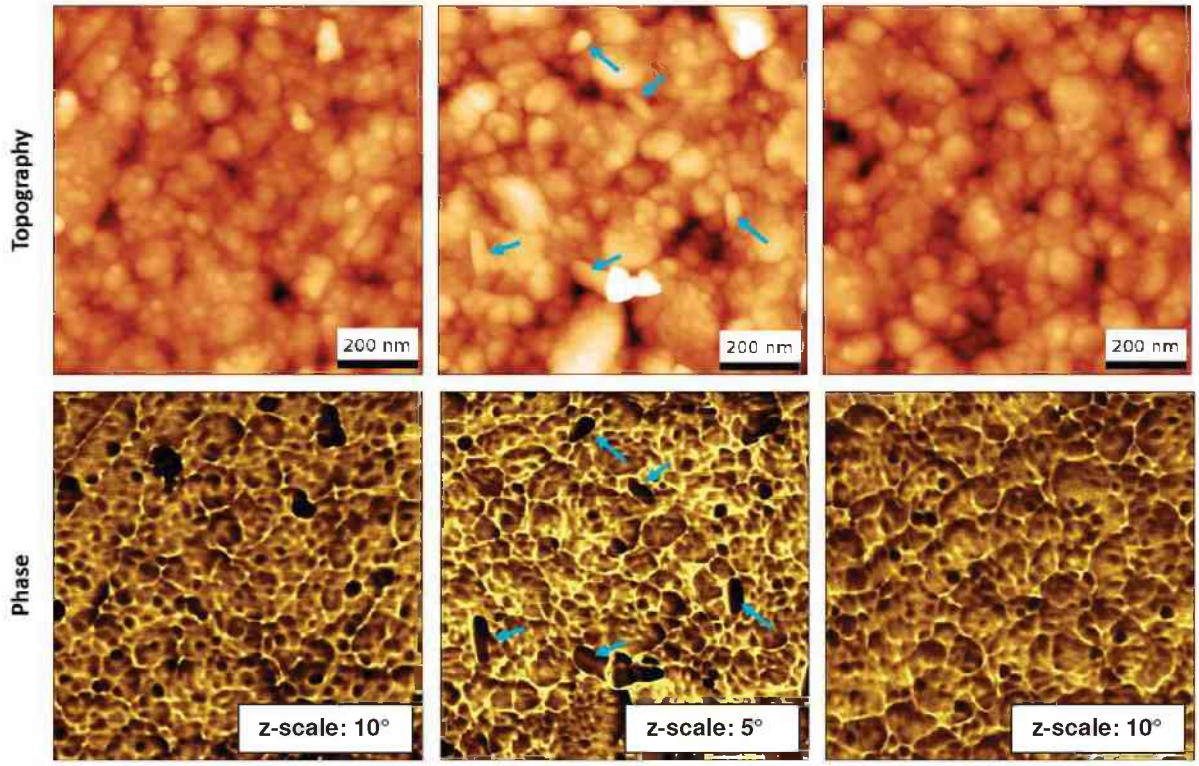

Figure 4.19: 1 x 1 µm² topography (z-scale: 25 nm) and phase (z-scale as indicated in the images) images of the pH=7, 8 and 9 samples, all without NaCl, recorded with CH_3-functionalized tips. The blue arrows in the images of pH=8 indicate areas with stronger phase contrast.

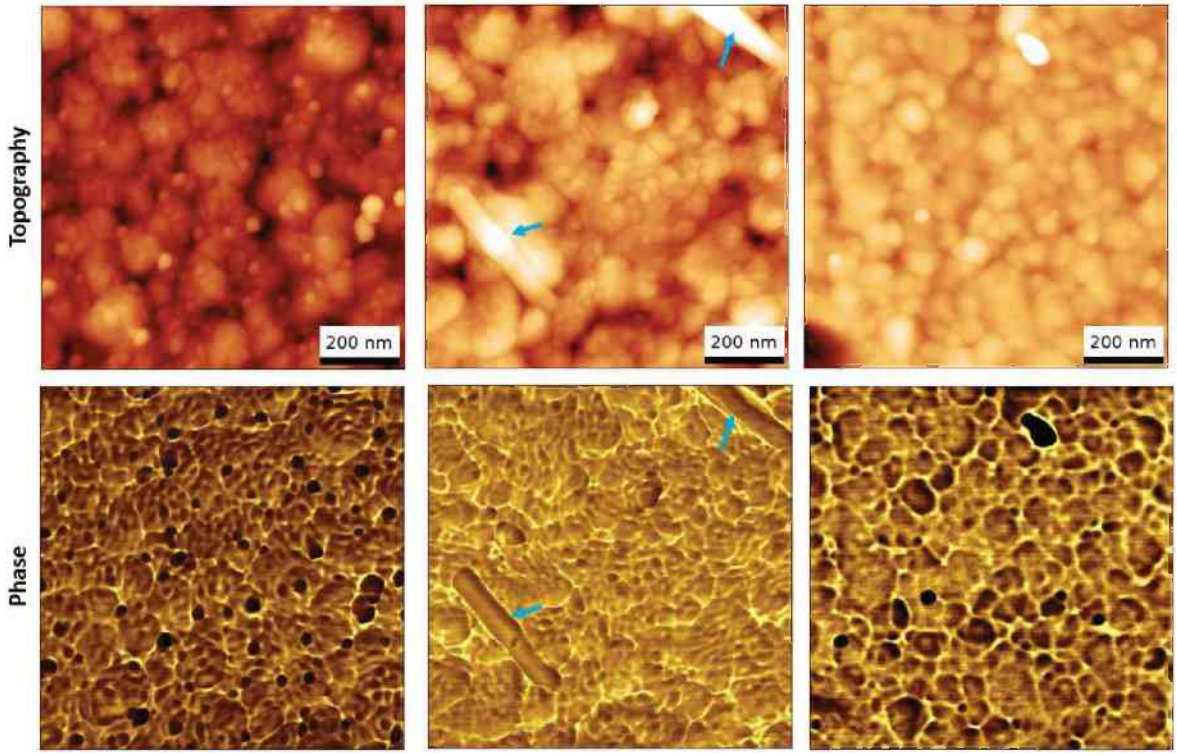

Figure 4.20: 1 x 1 µm² topography (z-scale: 30 nm) and phase (z-scale: 10°) images of the pH=7, 8 and 9 samples, all with 1 mmol NaCl, recorded with CH_3-functionalized tips. The blue arrows in the images of pH=8 indicate areas with stronger phase contrast.

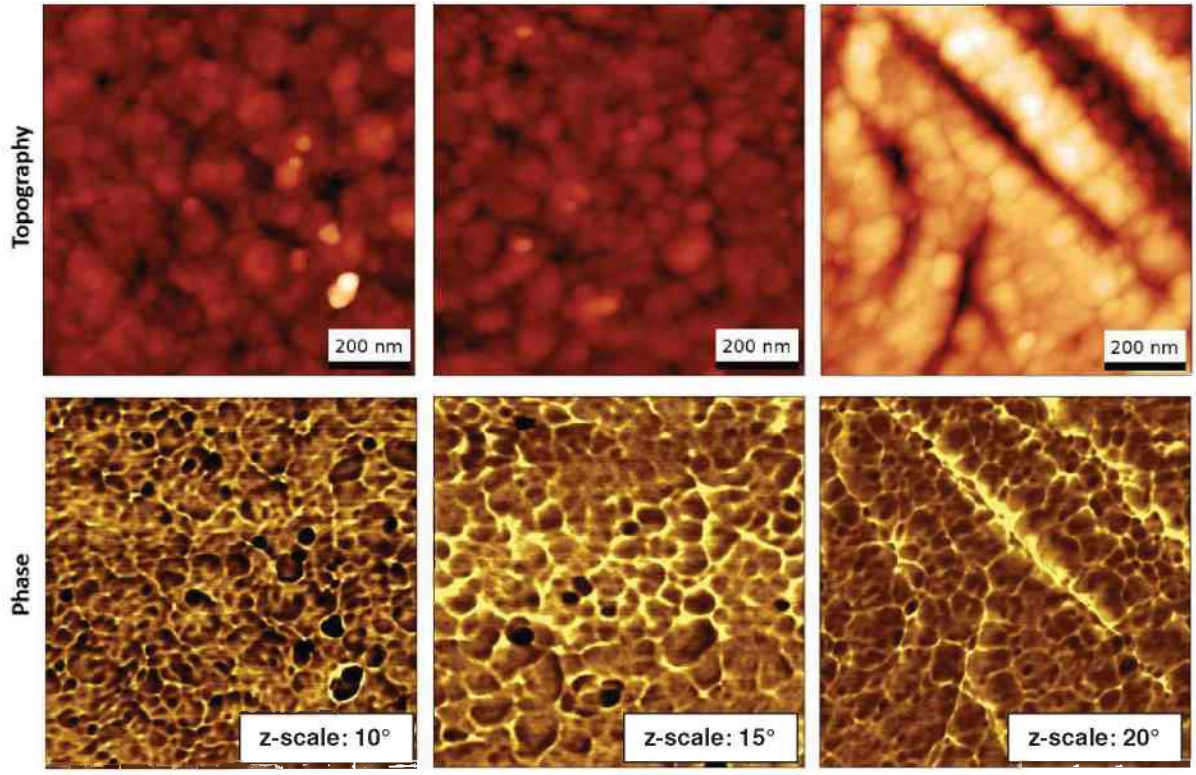

Figure 4.21: 1 x 1 µm² topography (z-scale: 40 nm) and phase (z-scale as indicated in the images) images of the pH=7, 8 and 9 samples, all with 100 mmol NaCl, recorded with CH_3-functionalized tips.

Images measured with CH_3-tips are more blurred and not as detailed as those recorded with OH-tips. However, OH-tips pick up contaminations more easily. This was not observed with CH_3-functionalized tips.

It is hard to distinguish between artifacts and real phase contrast. Especially for phase images measured with the OH-tips, the phase contrast is much smaller.

4.2.3 Force mapping

Since force mapping is more time consuming than phase imaging, only measurements on the pH=8 samples were performed. The setup was similar to the filtrated cellulose/xylan films described before, only the applied force was unintentionally increased to 70 nN. Here, OH- as well as CH_3-functionalized tips were used and the image size was always 500 x 500 nm^2 with 64 x 64 px.

In figures 4.22-24, the results obtained with the OH-functionalized tip are presented. Figures 4.25-27 display the force maps for the CH_3-functionalization. The blue markers in the topography images correspond to the yellow markers in the force maps. These areas were marked by using a masking tool in the Gwyddion software package. Since the marking was done manually, it should be noted that the resulting values are subject to bias. The yellow marking is shown here to display the lowest adhesion values compared to the unmarked region. It should be noted that not all the black regions are marked. This was done intentionally to sort out the locations with the lowest adhesion. In the phase contrast images, it seemed that xylan would adsorb randomly distributed on the surface and not cover the whole surface of the film. The averaged values for the marked and unmarked regions are listed in table 4.3.

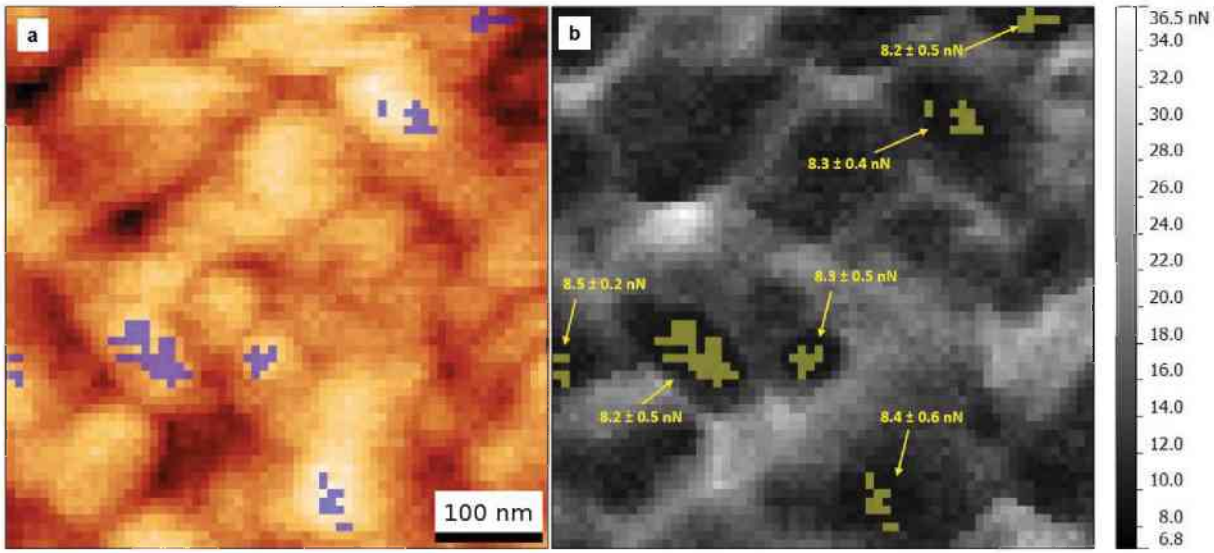

Figure 4.22: Maps of (a) topography (z-scale: 20 nm) and (b) adhesion force for the pH=8 sample without NaCl measured with the OH-functionalization.

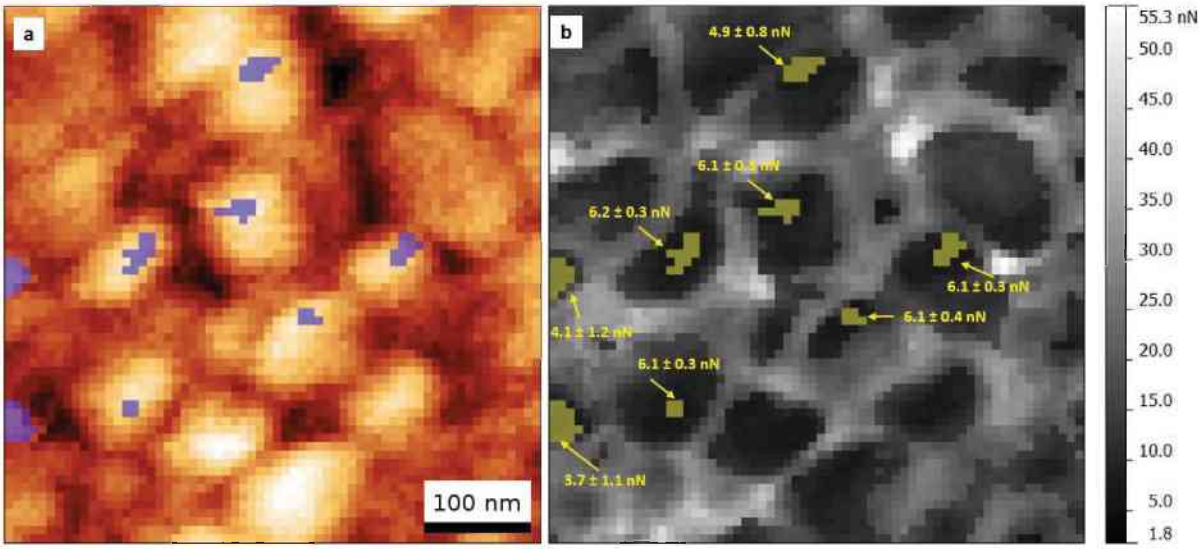

Figure 4.23: Maps of (a) topography (z-scale: 15 nm) and (b) adhesion force for the pH=8 sample with 1 mmol NaCl measured with the OH-functionalization.

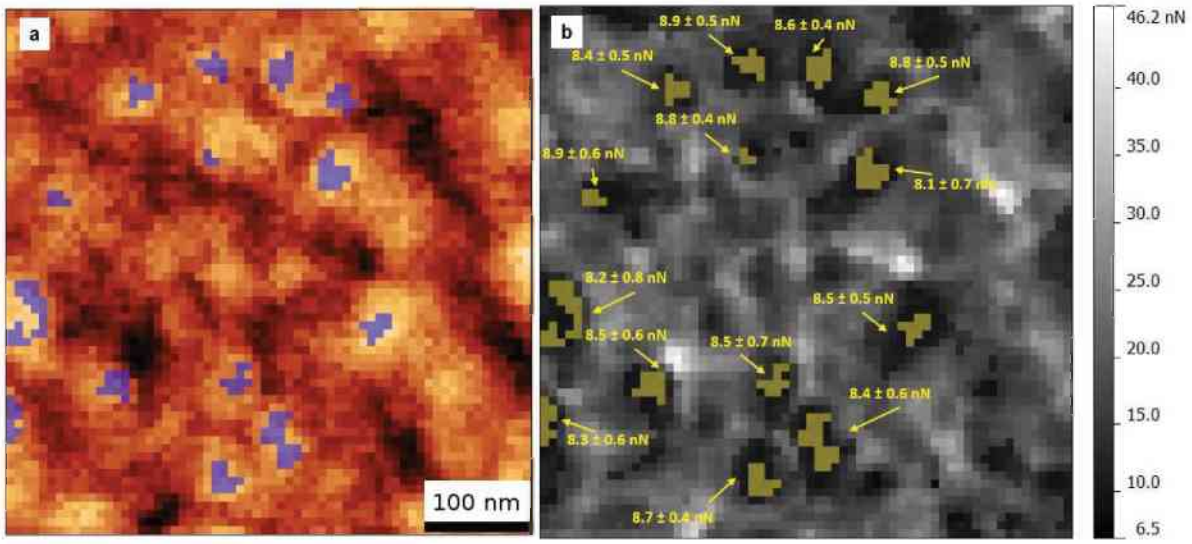

Figure 4.24: Maps of (a) topography (z-scale: 10 nm) and (b) adhesion force for the pH=8 sample with 100 mmol NaCl measured with the OH-functionalization.

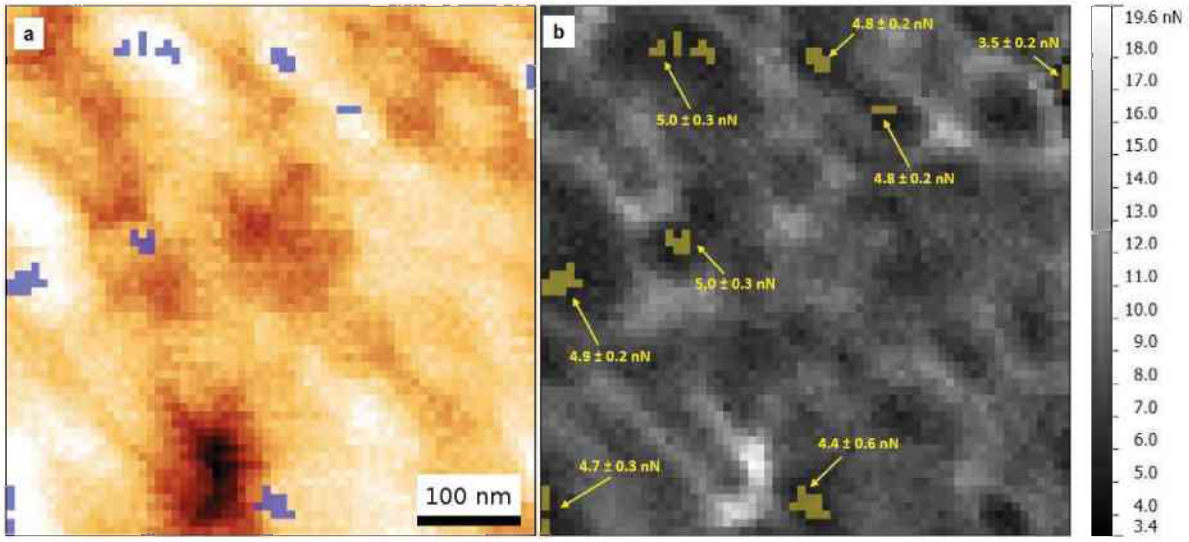

Figure 4.25: Maps of (a) topography (z-scale: 20 nm) and (b) adhesion force (z-scale: 16 nN) for the pH=8 sample without NaCl measured with the CH_3-functionalization.

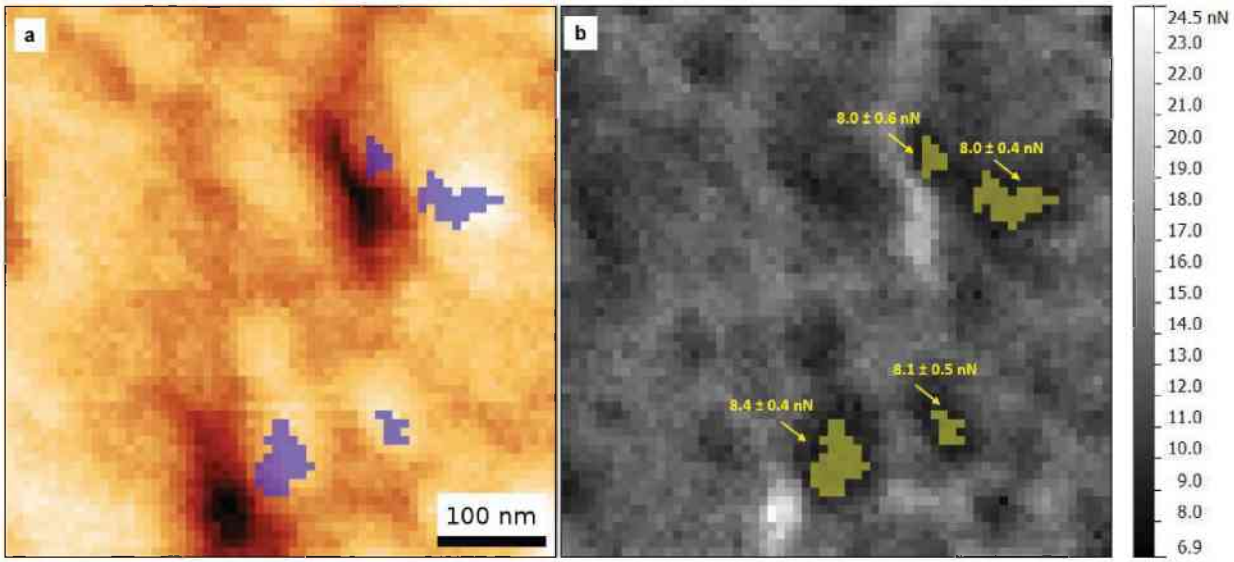

Figure 4.26: Maps of (a) topography (z-scale: 20 nm) and (b) adhesion force for the pH=8 sample with 1 mmol NaCl measured with the CH_3-functionalization.

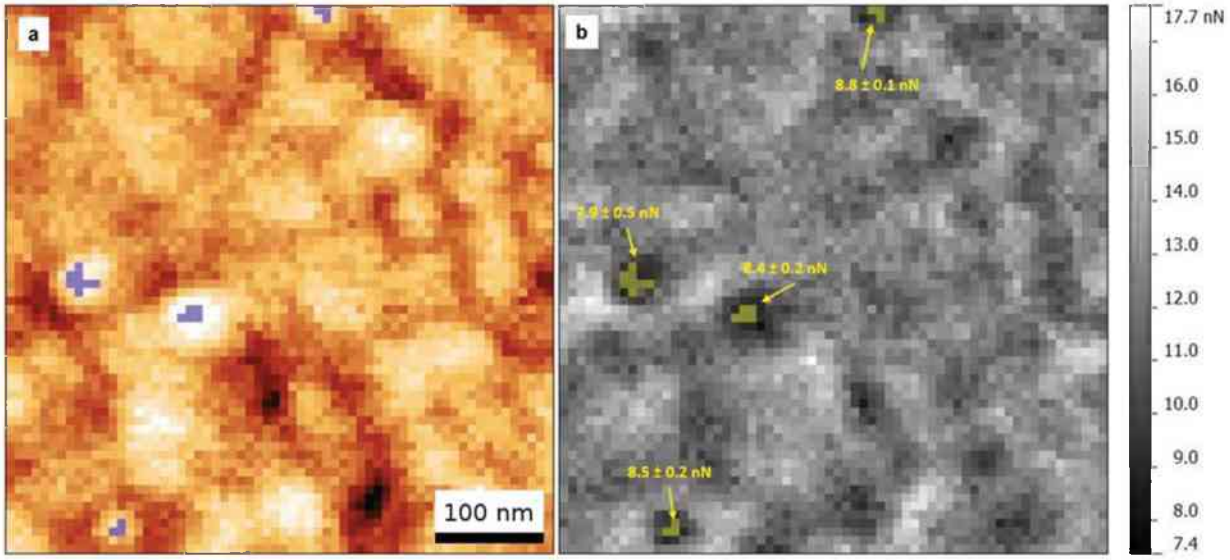

Figure 4.27: Maps of (a) topography (z-scale: 10 nm) and (b) adhesion force for the pH=8 sample with 100 mmol NaCl measured with the CH_3-functionalization.

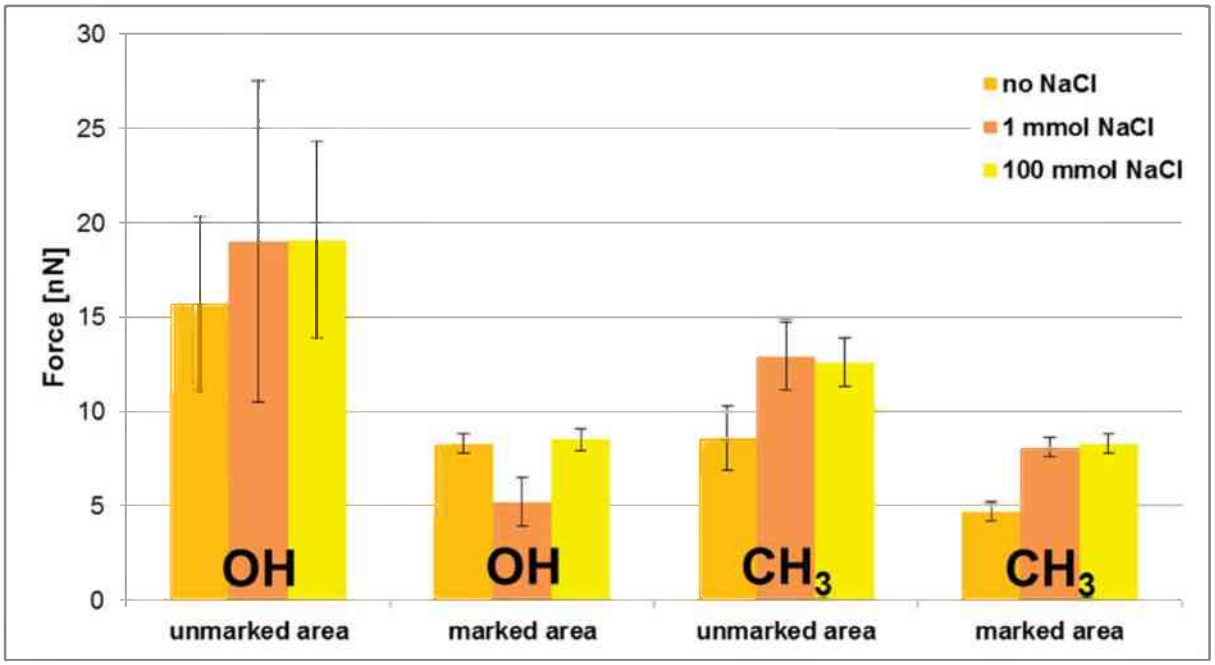

Figure 4.28: Averaged values for the adhesion force of the marked and unmarked areas on all pH=8 samples obtained from the force maps displayed in figures 4.22-27.

Since the observed contrast can be caused by either rests of NaCl, true chemical differences, and the topography, an interpretation of the results is difficult. However, from figure 4.28 it is clear that the adhesion force on surface regions which are suspected to be xylan are always around 5 nN to 9 nN. This fact indicated that there is no difference between OH and CH_3-tips, and the contrast is solely caused by the topography.

4.2.4 Summary

The results of the roughness analysis indicate that σ varies for different NaCl concentrations and different pH. The topography images also show that the surface structures are elongated, spherical or dot-like. Phase contrast was achieved with a hydrophilic OH- and a hydrophobic CH_3-functionalization but it was not possible to prove chemical contrast. Further it had been demonstrated that in force mapping, the influence of the topography is even more pronounced. Both tips, although different in chemical nature, obtain nearly the same adhesion force values on the surface regions which initially have been suspected to be xylan.

4.3 Paper fibers with adsorbed xylan

4.3.1 Roughness analysis

AFM measurements of the surface morphology of five different paper fiber samples were performed to detect a possible difference in xylan adsorption and distribution. The paper fibers were modified by adsorbing different xylans (X_1 and X_2) at different amounts (80 mg/g and 320 mg/g). As a reference sample, a paper fiber without xylan was also investigated. Further details on the xylans X_1 and X_2 can be found in chapter 3.

In figure 4.28 the 5 x 5 µm² topography images of all samples are shown, whereas figure 4.29 represents all 2 x 2 µm² topography scans.

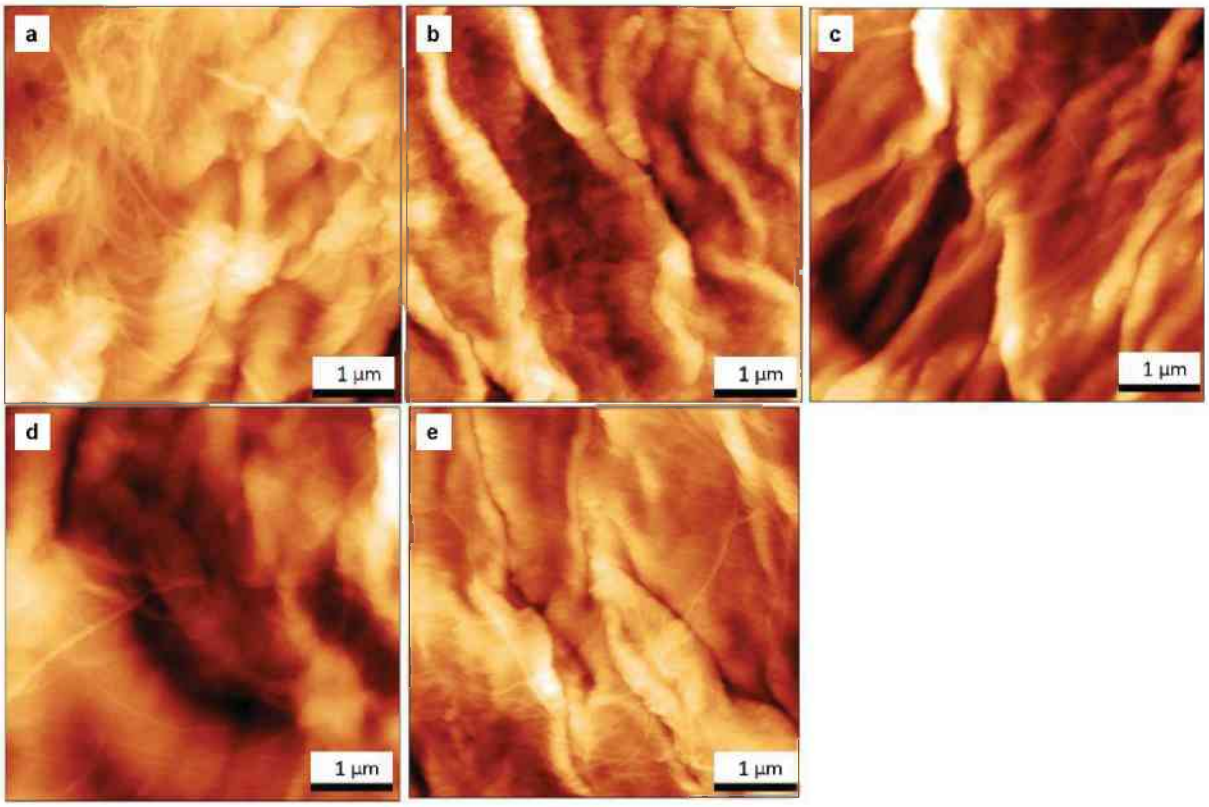

Figure 4.29: Representative 5 x 5 µm² topography images of all paper fiber samples: (a) reference (z-scale: 0.70 µm), (b) X_1-80 mg/g (z-scale: 0.40 µm), (c) X_1-320 mg/g (z-scale: 0.5 µm), (d) X_2-80 mg/g (z-scale: 0.60 µm) and (e) X_2-320 mg/g (z-scale: 0.50 µm).

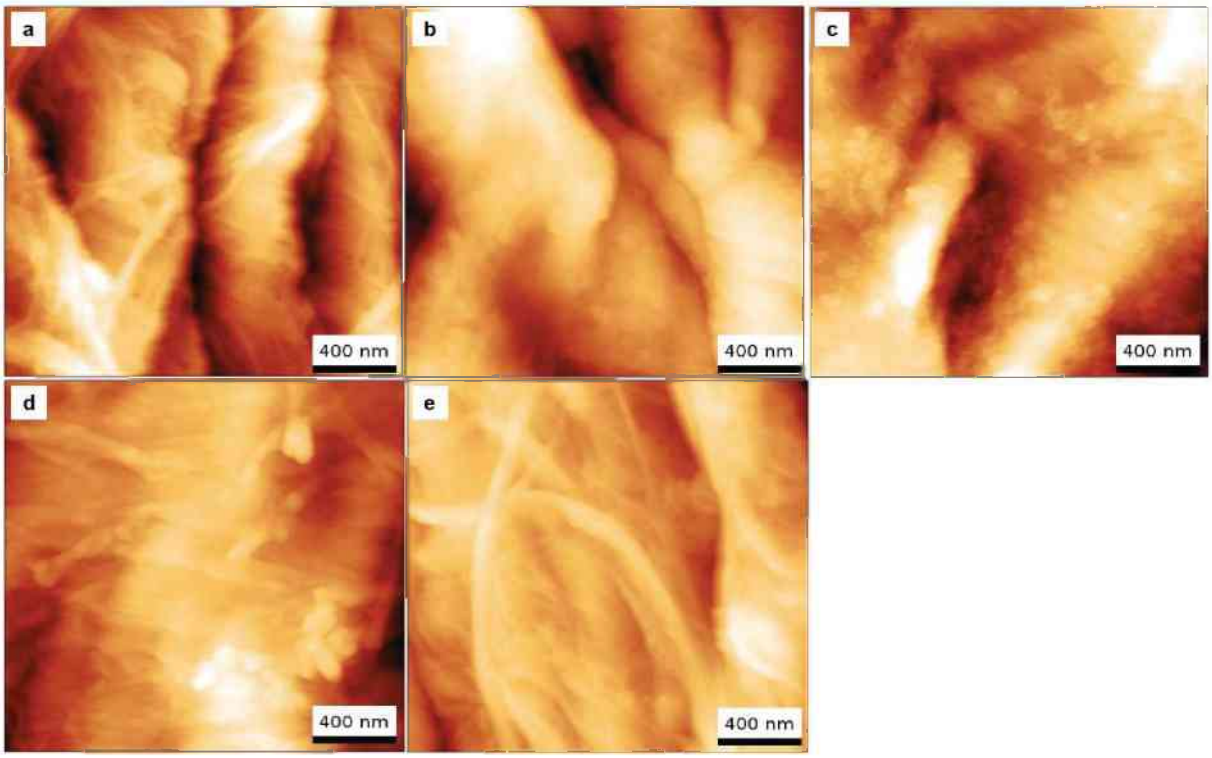

Figure 4.30: Representative 2 x 2 µm² topography images of all paper fiber samples: (a) reference (z-scale: 0.35 µm), (b) X_1-80 mg/g (z-scale: 0.45 µm), (c) X_1-320 mg/g (z-scale: 0.25 µm), (d) X_2-80 mg/g (z-scale: 0.25 µm) and (e) X_2-320 mg/g (z-scale: 0.50 µm).

The surface of all fiber samples looks wrinkled and microfibrils and fibril bundles are visible. Only on the topography images of the pulp fibers with X_1 xylan, features on the surface are visible which could be considered as adsorbed xylan. These nearly spherical features have a size of about 100 nm in diameter and are 20 nm – 30 nm high. The structures are not seen on the reference sample, but neither on the X_2 samples. Especially the topography scans of the reference sample and the X_2 composition samples look very similar.
The roughness analysis was performed on the 5 x 5 µm² topography images and the results for each roughness parameter are presented in figures 4.30-32.

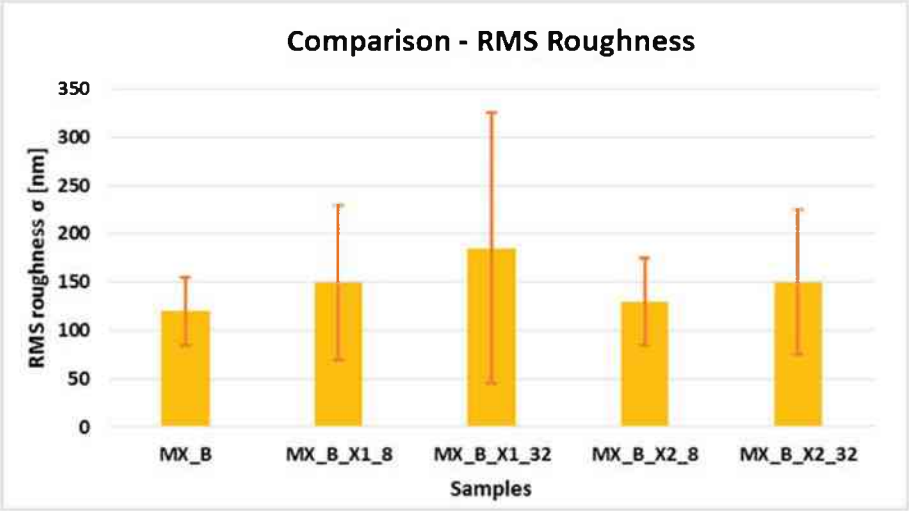

Figure 4.31: Comparison of the RMS roughness for all paper fiber samples.
MX_B = reference, MX_B_X1_8 = X_1-80 mg/g, MX_B_X1_32 = X_1-320 mg/g, MX_B_X2_8 = X_2-80 mg/g, MX_B_X2_32 = X_2-320 mg/g.

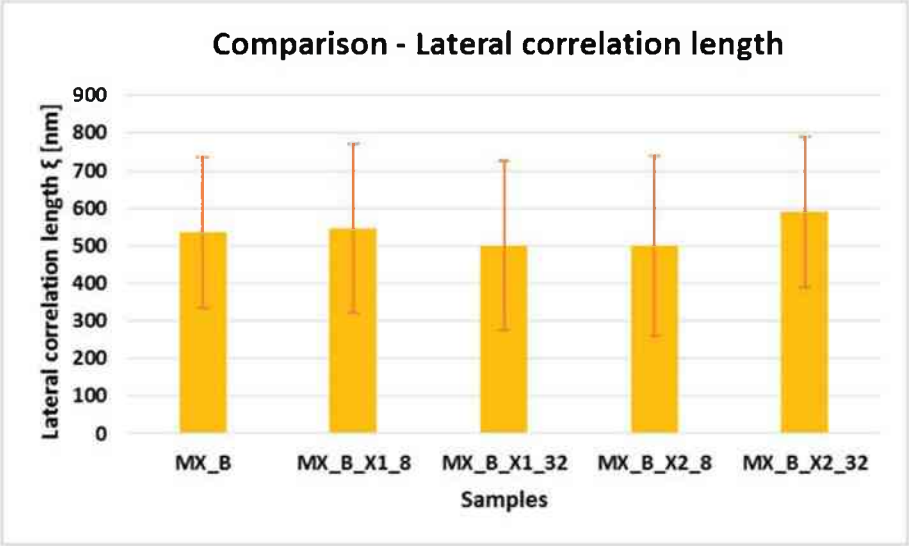

Figure 4.32: Comparison of the lateral correlation length for all paper fiber samples.
MX_B = reference, MX_B_X1_8 = X_1-80 mg/g, MX_B_X1_32 = X_1-320 mg/g, MX_B_X2_8 = X_2-80 mg/g, MX_B_X2_32 = X_2-320 mg/g.

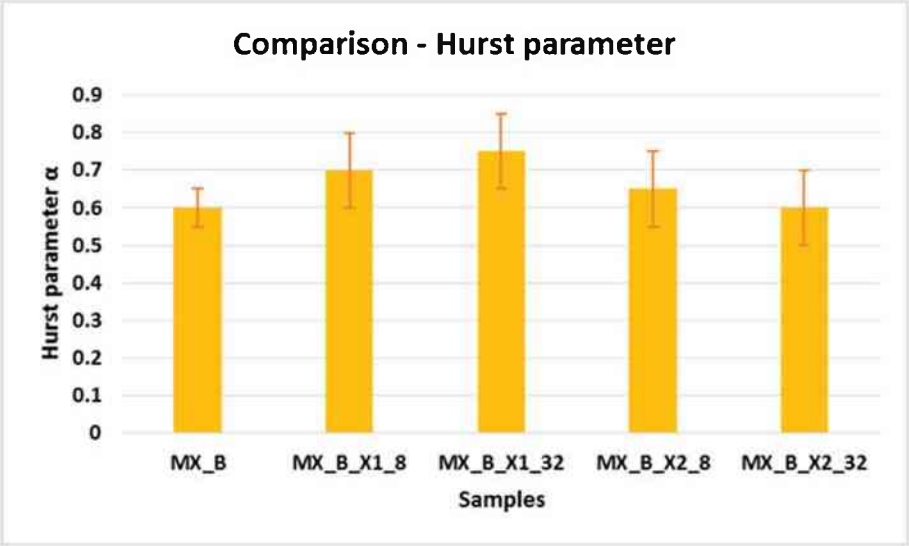

Figure 4.33: Comparison of the Hurst parameter for all paper fiber samples.
MX_B = reference, MX_B_X1_8 = X_1-80 mg/g, MX_B_X1_32 = X_1-320 mg/g, MX_B_X2_8 = X_2-80 mg/g, MX_B_X2_32 = X_2-320 mg/g.

It is visible that there is no significant difference in the values of the roughness parameters σ, ξ and α for all samples. This is mostly due to the very high roughness of the fibers themselves. Small features on the surface would not make a huge difference in the results compared to the fibers' overall roughness [46].
Eventually, it is not possible to find out for certain if the surface features are really xylan from the topography images.

4.3.2 Phase imaging

For phase imaging, 2 x 2 µm² and 500 x 500 nm² scans of the reference sample and the X_1-80 mg/g sample were recorded. Again, OH- and CH_3-functionalized probes were used. In figure 4.33-34 the results for the 500 x 500 nm² topography and phase images obtained with the OH-functionalized probes are shown. Figure 4.35-36 represents the 500 x 500 nm² scans recorded with a CH_3-modified tip.

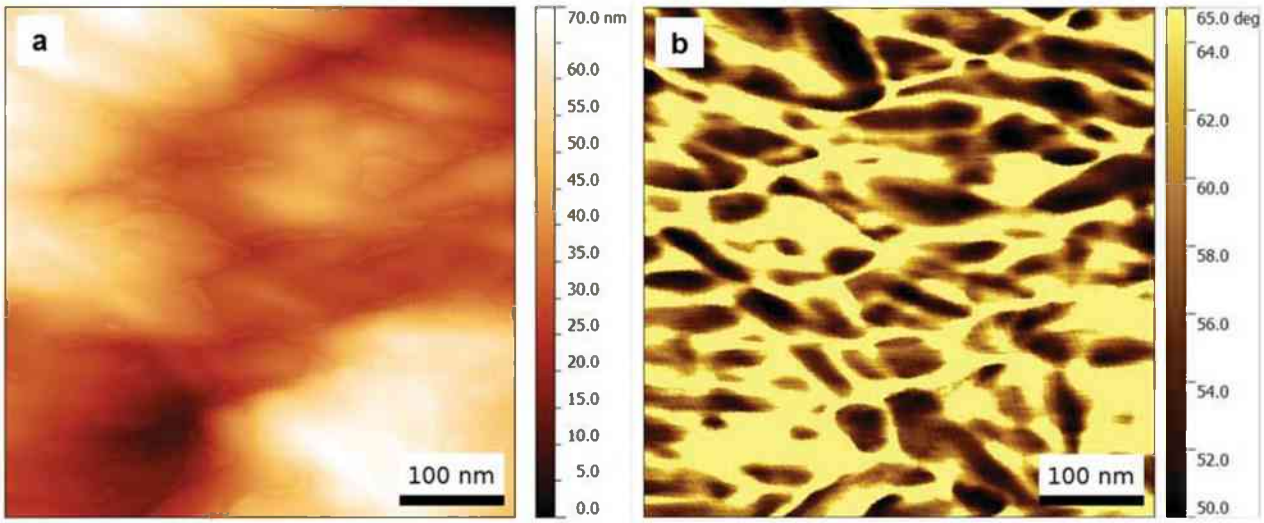

Figure 4.34: (a) Topography and (b) phase images obtained with OH-functionalization for the reference sample.

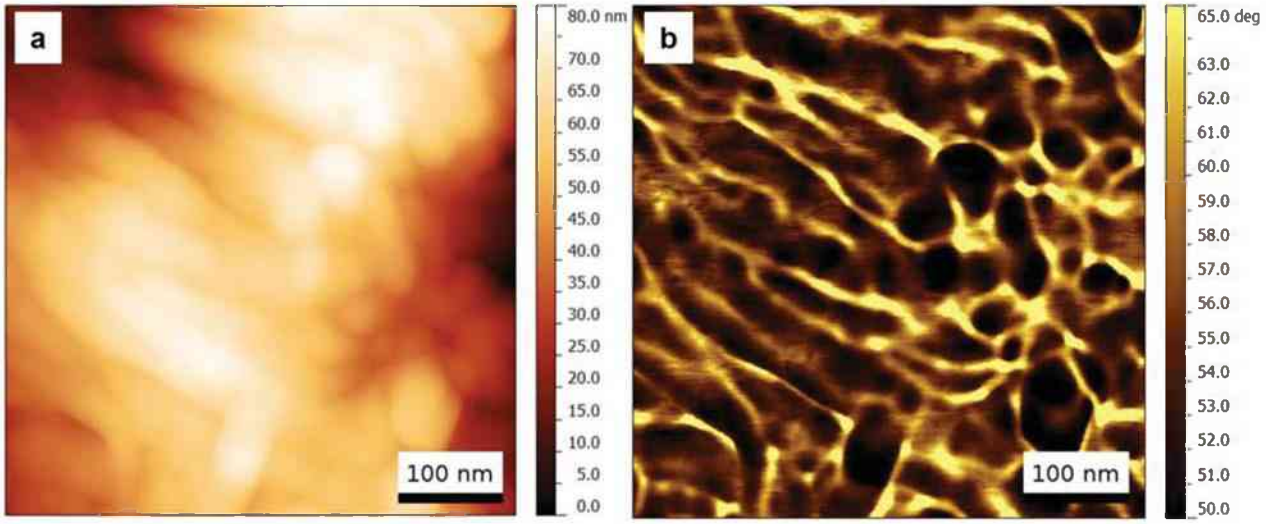

Figure 4.35: (a) Topography and (b) phase images obtained with OH-functionalization for the X_1-80 mg/g sample.

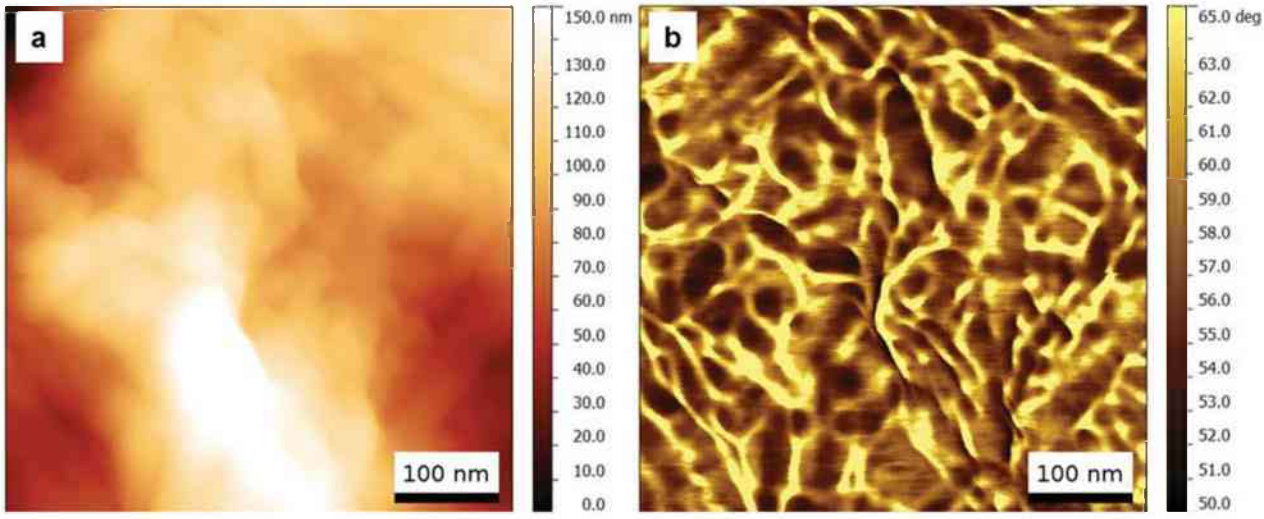

Figure 4.36: (a) Topography and (b) phase images obtained with CH_3-functionalization for the reference sample.

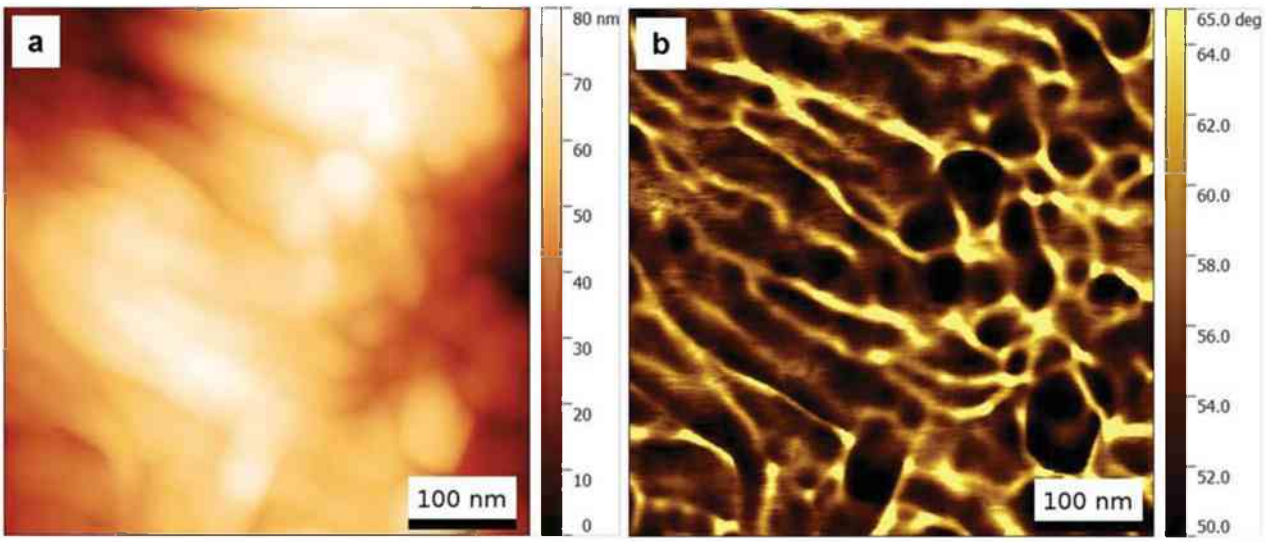

Figure 4.37: (a) Topography and (b) phase images obtained with CH_3-functionalization for the X_1-80 mg/g sample.

The phase contrast between the reference sample and the X_1-80 mg/g sample is clearer with the OH-functionalized probes. For the same range of degrees in phase, the reference sample shows little difference, but for the X_1-80 mg/g sample there is more contrast. This could be due to the hydrophilic nature of the OH-groups. In the valleys and pits of the fiber surface, more water is present than on hills, so there should be more interaction with the tip. This is also visible in figure 4.33 by comparing the topography and phase image.
For the CH_3-modification in figure 4.35-36, the phase contrast does not show any significant difference between the reference and the X_1-80 mg/g sample.

4.3.3 Force mapping

Again, OH- and CH_3-functionalization were used to obtain force maps for the reference and the X_1-80 mg/g sample. For the force mapping of paper fibers, lower forces than on the cellulose films were applied. The forces ranged between 3 and 10 nN. Otherwise the parameters were not changed compared to the previously shown force mapping results.
In figure 4.38-39, the force maps for the OH-functionalization and in figure 4.40-41 the force maps for the CH_3-modification are shown. Blue markings show corresponding areas in topography image and force map. The blue areas also indicate areas of low adhesion, which were again obtained by using the masking tool in the Gwyddion software package. In figure 4.42, the averaged values of the adhesion force for the marked and unmarked areas are compared.

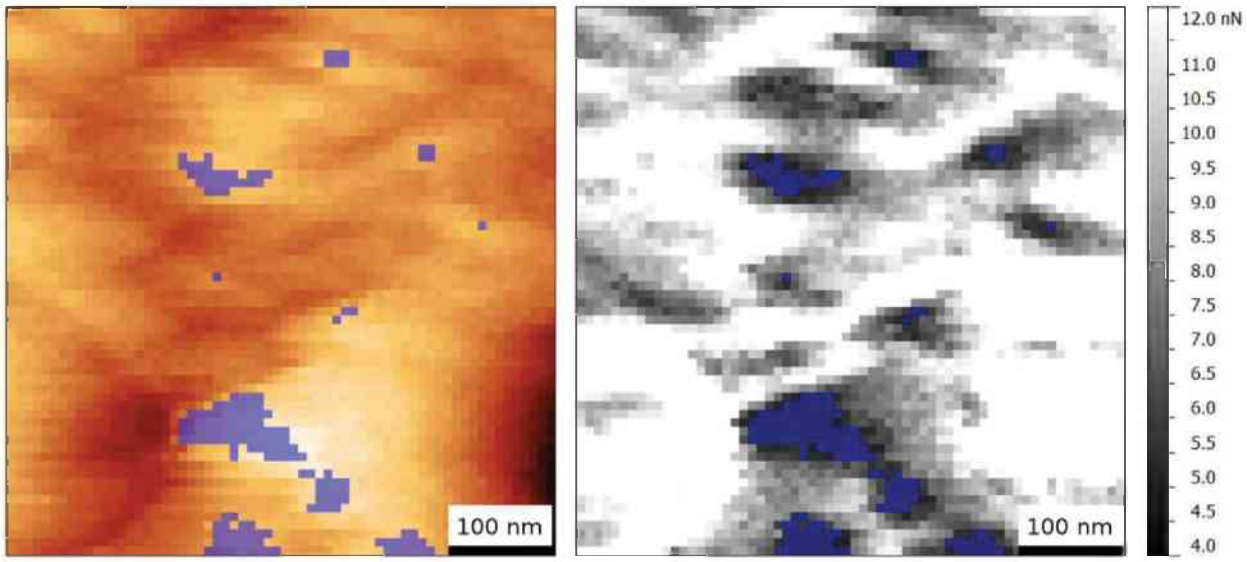

Figure 4.38: Topography (z-scale: 70 nm) and corresponding adhesion force maps obtained with the OH-functionalization for the reference sample.

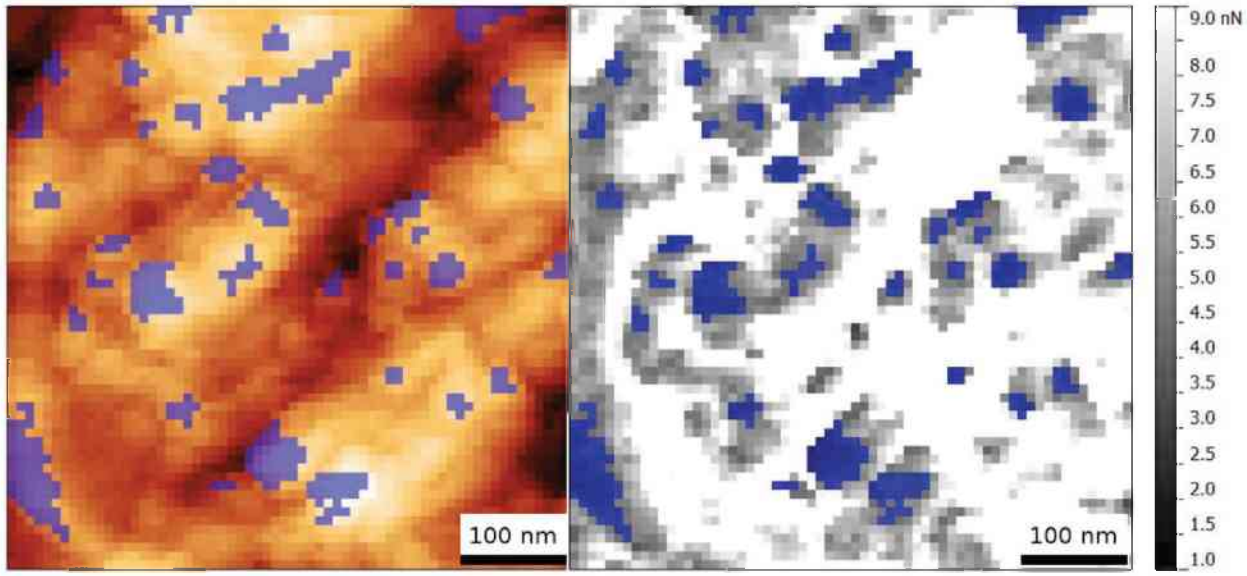

Figure 4.39: Topography (z-scale: 45 nm) and corresponding adhesion force maps obtained with the OH-functionalization for the X_1-80 mg/g sample.

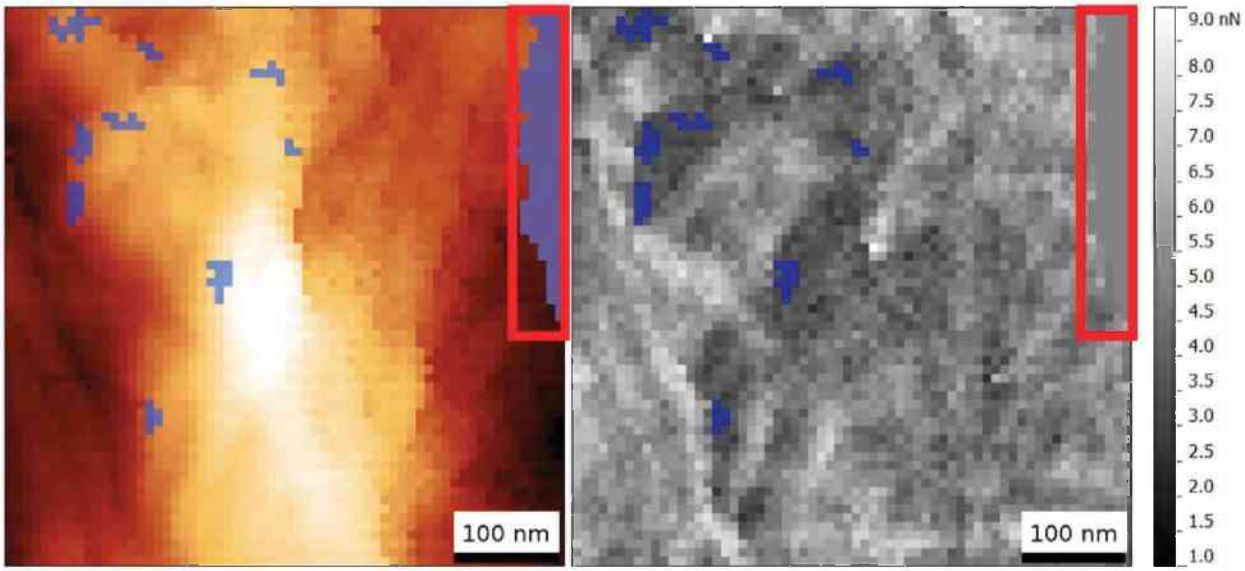

Figure 4.40: Topography (z-scale: 120 nm) and corresponding adhesion force maps (z-scale: 8 nN) obtained with the CH_3-functionalization for the reference sample. The red square with the blue marked region indicates an area were no force-distance curves were recorded due to high roughness.

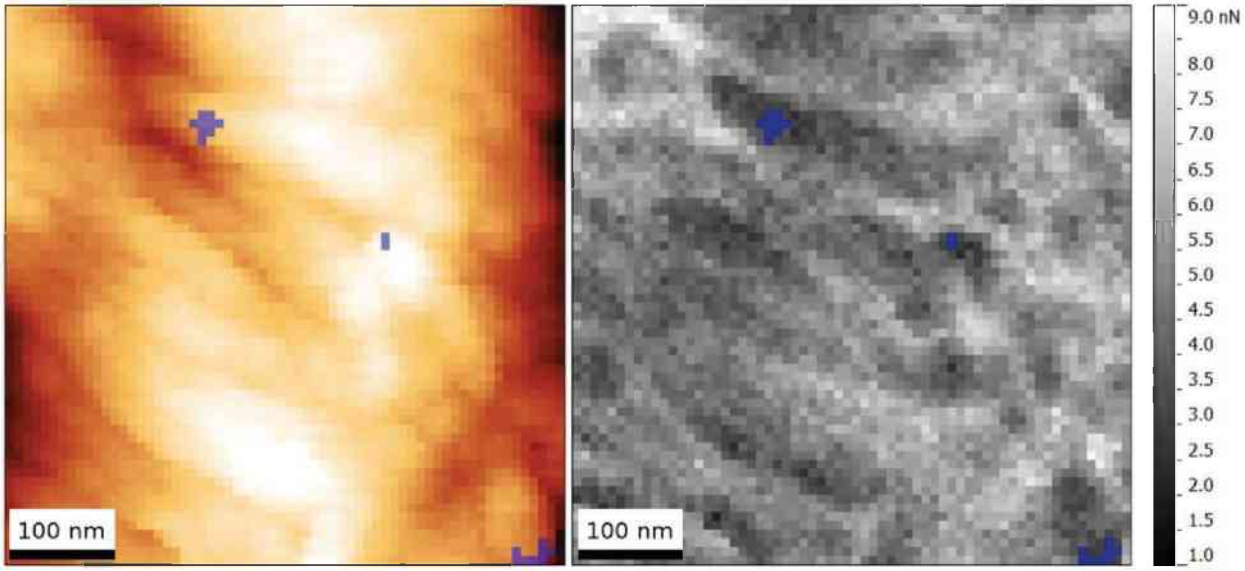

Figure 4.41: Topography (z-scale: 60 nm) and corresponding adhesion force maps (z-scale: 8 nN) obtained with the CH_3-functionalization for the X_1-80 mg/g sample.

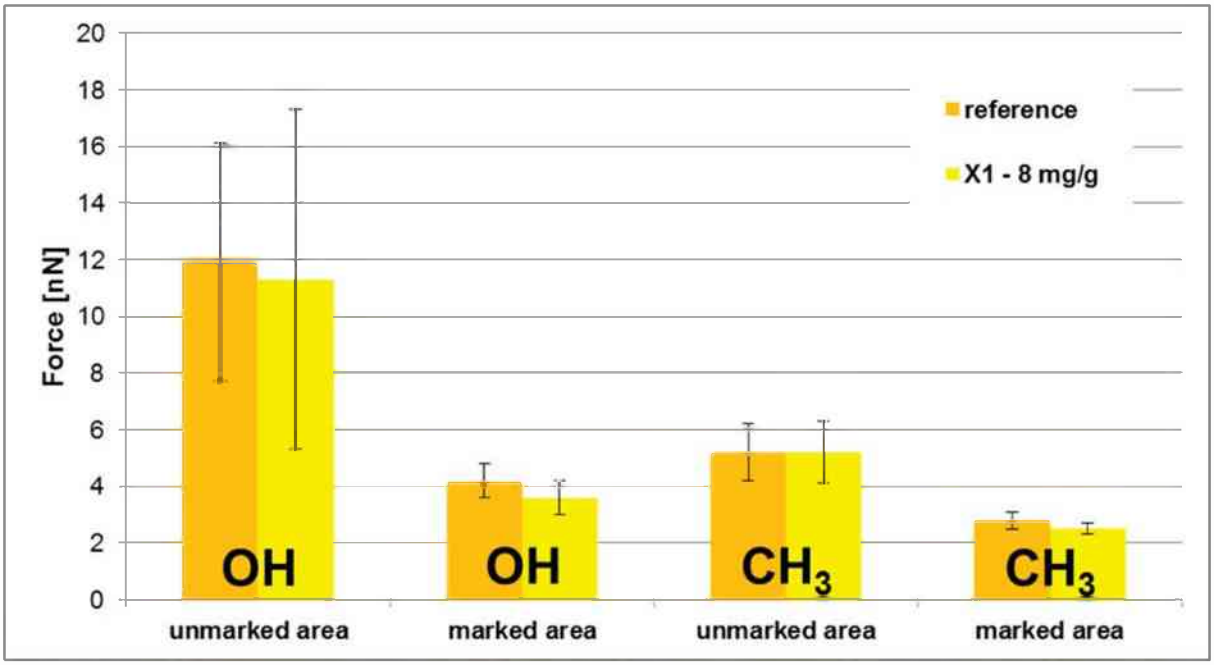

Figure 4.42: The averaged values of the adhesion of the marked and unmarked areas for both functionalizations.

Both functionalizations achieve a contrast in adhesion force on paper fiber surfaces. Circular areas with lower adhesion are frequently observed. For the OH-modified probe, the contrast is clearly higher. Due to its hydrophilic character it is sensitive to water which is located everywhere on the surface. Even in the force map of the reference sample, which should be nearly without xylan, areas of lower adhesion are visible. Using the results obtained from the cellulose/xylan films as a basis, one has again to assume that the areas with low adhesion forces are caused by the samples' topography.

4.3.4 Summary

For paper fibers with adsorbed xylan, the roughness parameters show no difference for the reference sample and the samples with adsorbed xylan. Only on the fibers with X_1, aggregates with lateral dimensions of about 100 nm were found. Both phase imaging and force mapping result in a contrast. Here, also the higher surface position shows lower phase contrast or adhesion force. Since the paper fibers are rougher than the films, the topography influence should be even more enhanced. Comparison between the two functionalizations, shows better contrast for the OH-modified probes. This is mostly due to its hydrophilic nature.

5 Conclusions and Outlook

Conclusions

In this work, atomic force microscopy has been used in a comprehensive way to study not only topography, but also to explore a method obtaining chemical contrast between cellulose and hemicellulose (xylan) on different cellulosic materials. By using functionalized AFM tips (hydrophilic OH and hydrophobic CH_3) in tapping mode, xylan was aimed to be identified on the surface by a distinct phase contrast. Additionally, the adhesion force of the tip to the surface was recorded by force mapping. Since paper fibers are an inhomogeneous and complicated system, the adsorption of xylan to cellulose model films was studied in a first step.

For two of four cellulose/xylan films, a "ChromaFil" 0.45 µm filter was used. In the topography measurements, 5 x 5 µm² and 1 x 1 µm² images were recorded and evaluated by a comprehensive roughness analysis. Here, almost no difference between the filtrated and unfiltrated samples was found, except the unfiltrated sample #2 has a higher RMS roughness σ. A likely explanation is that the filter removes larger contaminations, leading to a less rough surface. A phase contrast was seen between protrusions and background but it is very likely that the phase images were influenced by strong topography variations. The same was concluded for the results of the force mapping with OH-functionalized probes.

In another attempt, different model films were prepared on quartz-crystal-microbalance substrates and afterwards exposed to a solution of xylan with varying ionic strengths and pH. Here, the results of the roughness analysis of 1 x 1 µm² images indicated that σ varies for different NaCl concentrations and different pH values. The topography images showed elongated, spherical or dot-like surface structures. The elongated structures are located along the slope of the hills, but the other structures preferentially adsorbed on top of the film's hill-like structures. Phase contrast was achieved with both functionalization, but it was not possible to prove chemical contrast. For force mapping, the influence of the topography was found to be even more pronounced. Both tips, although different in chemical nature, yielded the same contrast on the surface regions which initially have been suspected to be xylan.

Paper fibers with adsorbed xylan have a much higher roughness than the model thin films, but comparing fibers with each other, the roughness parameters of the analyzed 5 x 5 µm² images showed no difference between the reference sample and the samples with adsorbed xylan. Only the topography images of the fibers with xylan X_1 show aggregates with lateral dimensions of about 100 nm. Although phase imaging and force mapping result in a contrast, the higher surface positions show lower phase contrast or adhesion force. Again, this signals

towards a topographic influence and since the paper fibers are rougher than the films, it is even more enhanced. If the hydrophilic and hydrophobic functionalizations are compared, the OH-modified probes show a better contrast due to the hydrophilic nature.
This work showed that an influence of topography cannot be neglected. It proved that chemical contrast with AFM methods is a complex topic and it is not possible to use it as an easy tool to detect differences between cellulose and xylan.

Outlook

After the experimental work was finished, collaborators at University of Technology Graz, who provided the cellulose thin film samples, found out that - contrary to what was believed before - the cellulose films are completely covered in adsorbed xylan. Thus, the investigated samples in this work are too rough to exclude topographic influence in the chemical AFM methods. These facts show that AFM should not be used exclusively for chemical investigations on the presented cellulose and xylan systems at the moment. To apply the chemical AFM methods on cellulose-xylan systems, probably more experimental simplification is needed. First, it needs to be assured that only chemical contrast is achieved in the measurements. This could be done with very smooth samples consisting of alternating zones of cellulose and xylan. This idea was already partially tested before the decision was made to try functionalized probes. Another more analytical approach would be to subtract the contact area from the measured adhesion force to obtain real adhesion values.
Making the chemical AFM methods work, especially force mapping, would be interesting because it could provide a combined measurement tool for chemical and viscoelastic properties. An accurate characterization of viscoelastic materials with AFM is interesting, but it is difficult due to the complexity of the material behavior – in this case paper fibers. The bulk behavior of viscoelastic materials is often represented with simple empiric models combining springs and dash pots, which are used at the continuum scale [47, 48]. Drawing a connection from continuum mechanics to AFM measurements is not as simple as it seems, and there is a need for the development of more physically accurate models that are able to describe nanoscale phenomena [49]. Therefore, it would be promising to combine different novel AFM based methods like bimodal AFM [48] and AFM nanomechanical mapping [50] for viscoelastic properties and to investigate and evaluate them for paper fibers, which have not been studied yet for the nanoscale effects of viscoelasticity.

Acknowledgments

For helping me in the course of this work I want to thank

Ao.Univ.-Prof. Dipl.-Phys. Dr.rer.nat. Christian Teichert for his kind and excellent supervision, for teaching me about AFM and more, for all the travels and conferences, for giving me the opportunity to work in the SPM Group and to write this thesis and the correction of this work. I am very happy that he was so relentless in persuading my shy soul to join his group and helping me find a direction in my life.

Dipl.-Ing. Dr.mont. Christian Ganser for teaching me AFM and cellulose stuff, for the excellent supervision, the kind and very patient support, correction of this work and fun times during travels and in the office. His very calm nature and way of thinking helped me a lot to get a little grip on the chaos in my brain.

Ao.Univ.-Prof. Mag. Dr.rer.nat. Robert Schennach, Graz University of Technology, and leader of the Christian Doppler Laboratory for "Surface Chemical and Physical Fundamentals of Paper Strength" for providing helpful information and support and the possibility to perform this work.

Msc Esther Schennach, Graz University of Technology, for administrative support in all things concerning the Christian Doppler Laboratory for “Surface Chemical and Physical Fundamentals of Paper Strength” and for nice girl talk.

Dipl.-Ing. Dr. Albrecht Miletzky, Graz University of Technology, for sample preparation and helpful discussions.

Dipl.-Ing. Siegfried Zöhrer, Graz University of Technology, for sample preparation and helpful discussions.

Mag.rer.nat. Dr.rer.nat. Stefan Spirk, Dipl.-Ing. Dr.techn. Ulrich Hirn, Dipl.-Ing. Dr.techn. Rene Eckhart, Dipl.-Ing. Dr.mont. Franz J. Schmied, Dipl.-Ing. Dr. Wolfgang Fischer, Dipl.-Ing. Dr.techn. Jussi Lahti, Dipl.-Ing. Leo Arpa, Dipl.-Ing. Dr. Johannes Leitner, Dr. Ingo Bernt and **Dipl.-Ing. Dr. Frederik Weber** for helpful discussions within the Christian Doppler Laboratory.

Dipl.-Ing. Dr.techn. Markus Kratzer for his help regarding AFM and analytical methods and for fun times at lunch and in Kiev and Berlin. Also, for being such a great person, but not wanting to realize it.

Ing. Heinz Pirker for his technical support.

Heide Kirchberger, Thomas Jud and **Magdalena Ottrin** for administrative support.

Mag.inz. Monika Mirkowska, Dipl.-Ing. Patrice Kreiml, Msc Benjamin Kaufmann, Jakob Genser, Michael Lasnik, Michael Huszar, Dipl.-Ing. Stefan Klima and **Dipl.-Ing. Quan Shen** for the nice and fun time in the office and during travels and a good working atmosphere.

Christian Doppler Research Society for financial support.

My sister Chiara, my mum and some of my family

My friends and colleagues

Bibliography

[1] A. Ebringerová and T. Heinze. Xylan and xylan derivatives - Biopolymers with valuable properties, 1: Naturally occurring xylans structures, isolation procedures and properties. *Macromol. Rapid Commun.* **21** (2000) 542–556.

[2] P. C. Kersavage. Moisture content effect on tensile properties of individual Douglas-fir latewood tracheids. *Wood Fiber* **5** (1973) 105–117.

[3] J. Schönberg, C. Oksanen, T. Suurnäkki, A. Kettunen and H. Buchert. The importance of xylan for the strength properties of spruce kraft pulp fibres. *Holzforschung* **55** (2001) 639–644.

[4] T. Oksanen, J. Buchert and L. Viikari. The role of hemiocelluloses in the hornification of bleached kraft pulps. *Holzforschung* **51** (1997) 355–360.

[5] H. Duchesne, I. Hult, E.-L. Molin, U. Daniel, G. Iversen and T. Lennholm. The influence of hemicellulose on fibril aggregation of kraft pulp fibres as revealed by FE-SEM and CP/MAS13C-NMR. *Cellulose* **8** (2001) 103–111.

[6] H. L. Spiegelberg. The effect of hemicelluloses on the mechanical properties of individual pulp fibers. *Tappi* **49** (1966) 388–396.

[7] A. Sjöholm, E. Gustafsson, K. Norman, E. Reitberger and T. Colmsjö. Fibre strength in relation to molecular weight distribution of hardwood kraft pulp: Degradation by gamma irradiation, oxygen/alkali or alkali. *Nord. Pulp Pap. Res. J.* **15** (2000) 326–332.

[8] A. Linder, R. Bergman, A. Bodin, and P. Gatenholm. Mechanism of assembly of xylan onto cellulose surfaces. *Langmuir* **19** (2003) 5072–5077.

[9] B. Cappella and G. Dietler. Force-distance curves by atomic force microscopy. *Surf. Sci. Rep.* **34** (1999) 1–104.

[10] R. L. Crawford. *Lignin biodegradation and transformation*. New York: John Wiley and Sons, 1981.

[11] D. Klemm, B. Heublein, H. P. Fink, and A. Bohn. Cellulose: Fascinating biopolymer and sustainable raw material. *Angewandte Chemie - International Edition* **44** (2005) 3358–3393.

[12] Cellulose. *Wikipedia*. [Online].
Available: en.wikipedia.org/wiki/Cellulose. [Accessed: November 2015].

[13] H. Sixta. *Handbook of Pulp*, vol. 1–2. New York: John Wiley and Sons, 2008.

[14] A. Miletzky. Adding value to cellulose fibers by the addition of xylan. PhD thesis, Graz University of Technology, 2014.

[15] Xylan. *Wikipedia*. [Online].
Available: en.wikipedia.org/wiki/Xylan. [Accessed: November 2015].

[16] D. Fengel and G. Wegener. *Wood: chemistry, ultrastructure, reactions.* New York: John Wiley and Sons, 1984.

[17] R. E. Booker and J. Sell. The nanostructure of the cell wall of softwoods and its functions in a living tree. *Holz als Roh- und Werkst.* **56** (1998) 1–8.

[18] D. Clayton and J. Stone. The redeposition of hemicelluloses during pulping. Part I: The use of tritium-labeled xylan. *Pulp. Pap. Mag. Can.* **64** (1963) T459–T468.

[19] G. Ström, P. Barla, and P. Stenius. The effect of pine xylan on the use of some polycations as retention and drainage aids. *Svensk. Papperstidn.* **85** (1982) R100–R106.

[20] V. A. Russo. Sorption studies of a modified locust beam gum on a bleached sulfite pulp. PhD thesis, Appleton, Wisconsin, 1959.

[21] J. A. Hansson and N. Hartler. Sorption of hemicelluloses on cellulose fibers. Part 1: Sorption of xylans. *Svensk. Papperstidn.* **72** (1969) 521–530.

[22] M. Mitikka-Eklund. Sorption of xylans on cellulose fibers. Licentiate thesis, Helsinki University of Technology, 1996.

[23] G. Binnig, C. F. Quate and C. Gerber. Atomic force microscope. *Phys. Rev. Lett.* **56** (1986) 930.

[24] Q. Zhong, D. Inniss, K. Kjoller and V. B. Elings. Fractured polymer/silica fiber surface studied by tapping mode atomic force microscopy. *Surf. Sci.* **290** (1993) 1–206.

[25] J. Tamayo and R. García. Relationship between phase shift and energy dissipation in tapping-mode scanning force microscopy. *Appl. Phys. Lett.* **73** (1998) 2926–2928.

[26] P. Eaton and P. West, *Atomic Force Microscopy*. Oxford: Oxford University Press, 2010.

[27] D. Nečas and P. Klapetek. Gwyddion: an open-source software for SPM data analysis. *Open Phys.*, **10** (2012) 181–188.

[28] C. Teichert. Self-organization of nanostructures in semiconductor heteroepitaxy. *Physics Report*, **365** (2002) 335–432.

[29] Y. Zhao, G. Wang and T. Lu, *Characterization of amorphous and crystalline rough surface: principles and applications*. San Diego: Academic Press, 2001.

[30] S. K. Sinha, E. B. Sirota and S. Garoff. X-ray and neutron scattering from rough surfaces. *Phys. Rev. B* **38** (1988) 2297–2311.

[31] S. Rohm, U. Hirn, C. Ganser, C. Teichert and R. Schennach. Thin cellulose films as a model system for paper fiber bonds. *Cellulose* **21** (2014) 237–249.

[32] Mondi Products. [Online]. Available: http://www.mondigroup.com/products/desktopdefault.aspx/tabid-160. [Accessed: October 2015].

[33] W. J. Fischer, A. Zankel, C. Ganser, F. J. Schmied, H. Schroettner, U. Hirn, C. Teichert, W. Bauer and R. Schennach. Imaging of the formerly bonded area of individual fibre to fibre joints with SEM and AFM. *Cellulose* **21** (2014) 251–260.

[34] C. B. Babcock and K.L. Prater. Phase Imaging: Beyond Topography. *Veeco Application Note*, 1995.

[35] J. Tamayo and R. García. Deformation, Contact Time, and Phase Contrast in Tapping Mode Scanning Force Microscopy. *Langmuir* **12** (1996) 4430–4435.

[36] D. R. Baselt and J. D. Baldeschwieler. Imaging spectroscopy with the atomic-force microscope. *J. Appl. Phys.* **76** (1994) 33–38.

[37] GetRealTM Automated Probe Calibration. *Asylum Research Application Note*, 2014.

[38] J. L. Hutter and J. Bechhoefer. Calibration of Atomic-force microscopy tips. *Rev. Sci. Instrum.* **64** (1993) 1868.

[39] J. E. Sader, J. W. M. Chon and P. Mulvaney. Calibration of rectangular atomic force microscope cantilevers. *Rev. Sci. Instrum.* **70** (1999) 3967–3969.

[40] F. J. Schmied, C. Teichert, L. Kappel, U. Hirn and R. Schennach. Joint strength measurements of individual fiber-fiber bonds: An atomic force microscopy based method. *Rev. Sci. Instrum.* **83** (2012) 1–8.

[41] Asylum Research Probe Store. [Online].
Available: http://www.asylumresearch.com/ProbeStore. [Accessed: October 2015].

[42] S. Akari, D. Horn, H. Keller and W. Schrepp. Chemical Imaging by Scanning Force Microscopy. *Adv. Mater.* **7**(1995) 549–551.

[43] S. Zöhrer. Xylan Adsorption on Thin Cellulose Model Films. Master thesis, Graz University of Technology, 2014.

[44] J. Asunción. *The Complete Book of Papermaking*. New York: Lark Books, 2003.

[45] A. Miletzky, M. Punz, A. Zankel, S. Schlader, C. Czibula, C. Ganser, C. Teichert, S. Spirk, S. Zöhrer, W. Bauer and R. Schennach. Modifying cellulose fibers by adsorption/precipitation of xylan. *Cellulose* **22** (2015) 189–201.

[46] A. Miletzky, W. J. Fischer, C. Czibula, C. Teichert, W. Bauer and R. Schennach. How xylan effects the breaking load of individual fiber-fiber joints and the single fiber tensile strength. *Cellulose* **22** (2015) 849–859.

[47] E. A. López-Guerra and S. D. Solares. Modeling viscoelasticity through spring–dashpot models in intermittent-contact atomic force microscopy. *Beilstein J. Nanotechnol.* **5** (2014) 2149–2163.

[48] S. D. Solares. Probing viscoelastic surfaces with bimodal tapping-mode atomic force microscopy: Underlying physics and observables for a standard linear solid model. *Beilstein J. Nanotechnol.* **5** (2014) 1649–1663.

[49] S. D. Solares. Nanoscale effects in the characterization of viscoelastic materials with atomic force microscopy: coupling of a quasi-three-dimensional standard linear solid model with in-plane surface interactions. *Beilstein J. Nanotechnol.* **7** (2016) 554–571.

[50] Q. Guo. *Polymer Morphology: Principles, Characterization, and Processing*. New York: John Wiley and Sons, 2016.